Politecnico di Milano

SCHOOL OF INDUSTRIAL AND INFORMATION ENGINEERING

Master of Science – Energy Engineering

POLITECNICO
MILANO 1863

Modeling and Techno-Economic Assessment for Solid Oxide Electrolyzer Integration in a DRI Production Plant for Steel Industry Decarbonization

Advisor
Prof. Romano Matteo Carmelo

Co–advisor
Prof. Scaccabarozzi Roberto

Author
Capasso Stefano
ID: 968960

Academic Year 2024–2025

Abstract

Developing low-carbon production routes for primary ironmaking is essential to meet the ambitious CO_2 emission reduction targets of the steel sector. This work presents a detailed technical and economic assessment of a Direct Reduced Iron (DRI) production pathway, where the conventional natural gas reformer of a MIDREX process is replaced by a high temperature Solid Oxide Electrolyzer Cell (SOEC) for hydrogen production.

The reference natural gas based MIDREX plant and the alternative H_2-DRI configuration with integrated SOEC are modeled and rigorously compared using Aspen Plus under shared boundary conditions. The analysis focuses on the DRI production section, maintaining consistent shaft furnace operation to highlight the impact of the reducing gas generation technology.

The results demonstrate that the SOEC based route drastically reduces specific natural gas consumption and cuts direct CO_2 stack emissions by approximately 95% compared to the conventional process. This deep decarbonization is achieved while maintaining a high metallization degree, although with a lower DRI carbon content. The transition shifts the primary energy vector from fossil fuel to electricity, significantly increasing the plant's power demand.

A comprehensive economic assessment shows that the H_2-DRI configuration leads to significantly higher capital and operating expenditures, primarily due to the cost of the electrolyzer unit and increased electricity consumption. Consequently, the levelized cost of DRI production is substantially higher than for the natural gas route, resulting in a notable cost for CO_2 avoided. A long term scenario and sensitivity analysis show that the economic feasibility of the hydrogen route is predominantly governed by operational costs. Its competitiveness is therefore primarily governed by the availability of lower electricity prices and the implementation of higher carbon taxes, while a reduction in SOEC capital cost, though beneficial, has a comparatively lesser impact.

In conclusion, while SOEC integration enables a technically viable and deeply decarbonized DRI production route, its current economic attractiveness is limited. The analysis quantifies the clear trade-off between environmental performance and production cost, identifying the specific market and policy conditions under which hydrogen based ironmaking can become a competitive pillar for green steel.

Summary

List of Figures

List of Tables

1 Steelmaking Overwiev

The steel industry is one of the pillars of the global economy, ranking third worldwide in terms of material production by volume, after cement and timber, with an annual crude steel output of about 1,8 - 2,0 billion tonnes [1][2]. This scale, however, comes at a significant cost in terms of energy consumption and greenhouse gas emissions. Indeed, the sector is currently responsible for around 8% of global final energy demand and about 7% of energy sector CO_2 emissions, including process emissions. [2].

Considering its scale and environmental footprint, it is crucial to analyse how steel is produced in order to understand which stages of the process offer the greatest potential for reducing energy consumption and CO_2 emissions.

This section provides a general overview of the ironmaking and steelmaking industry. After brief definitions of iron and steel, it presents key global indicators (production, regional distribution, end-use sectors) together with data on the sector's energy demand and CO_2 intensity. Then the main steelmaking routes are briefly outlined, focusing on the principal processes that are described in Sections 1.1-1.3.

In general, "Iron" denotes the chemical element in its pure form, but also carbon-saturated intermediate (e.g. pig iron) and final (e.g. cast iron) products in the iron and steel sector. "Steel" denotes an alloy of iron and carbon, of which "carbon steel" is the simplest and most common variety. Although it can contain up to around 2% carbon by weight, the majority of carbon steels contain less than 0,25% carbon. More other elements (such as chromium, nickel, molybdenum, manganese etc...) are added to form more complex steel alloys, augmenting or diminishing certain physical properties for a given application [2].

The ability of steel to deform both elastically and plastically, and the high tensile strenght makes it the natural choice for many structural applications. In Figure 1-1 it is shown the share of steel percentage used by sector [3].

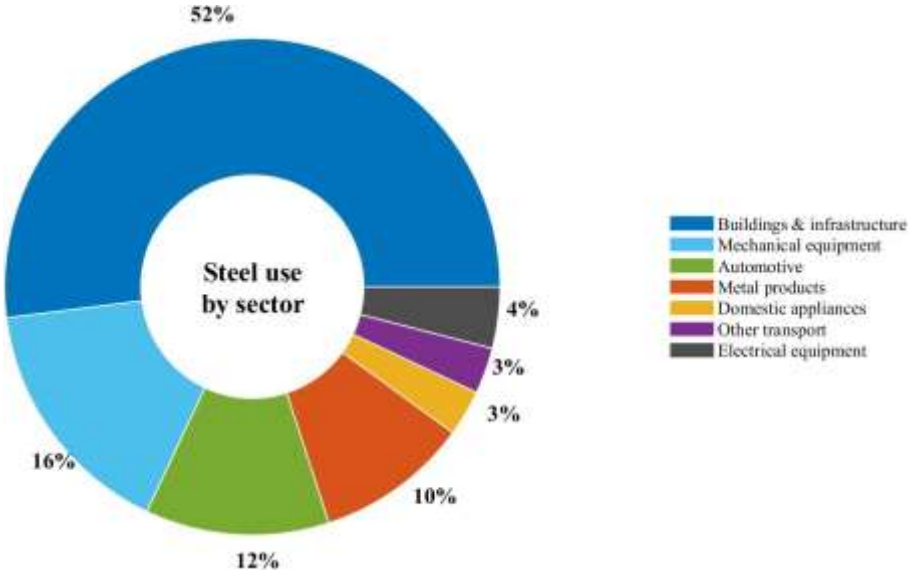

Figure 1-1. Steel use by sector

The main sector is related to buildings and infrastructure with 52% share, followed by mechanical equipment and automotive, respectively with 16% and 12%. These shares indicate that steel consumption is concentrated in sectors where materials must combine high reliability with a versatile property profile.

Looking at global output, as shown in Figure 1-2, crude steel production in 2024 is about 1885 million tonnes, with China the largest producer with about 1005 Mt (53,3% of the total), followed by India with 149,4 Mt and Japan 84 Mt [1]. The share by country is reported in Figure 1-2, based on crude steel production production of 2024 [1].

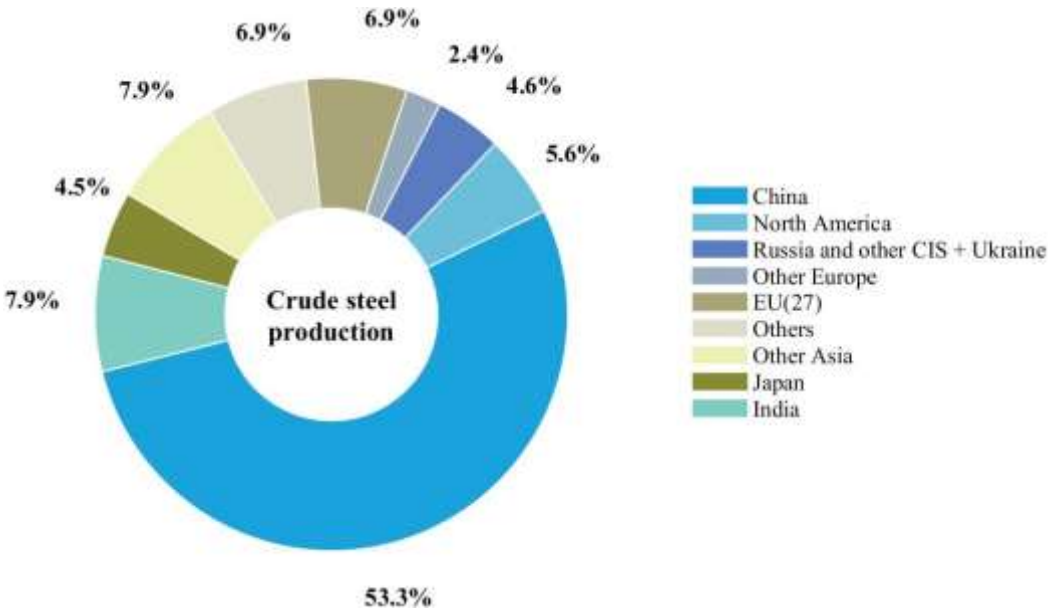

Figure 1-2. Countries share of crude steel production

Further Figure 1-3 highlights the crude steel production over the years, from the half of the last century.

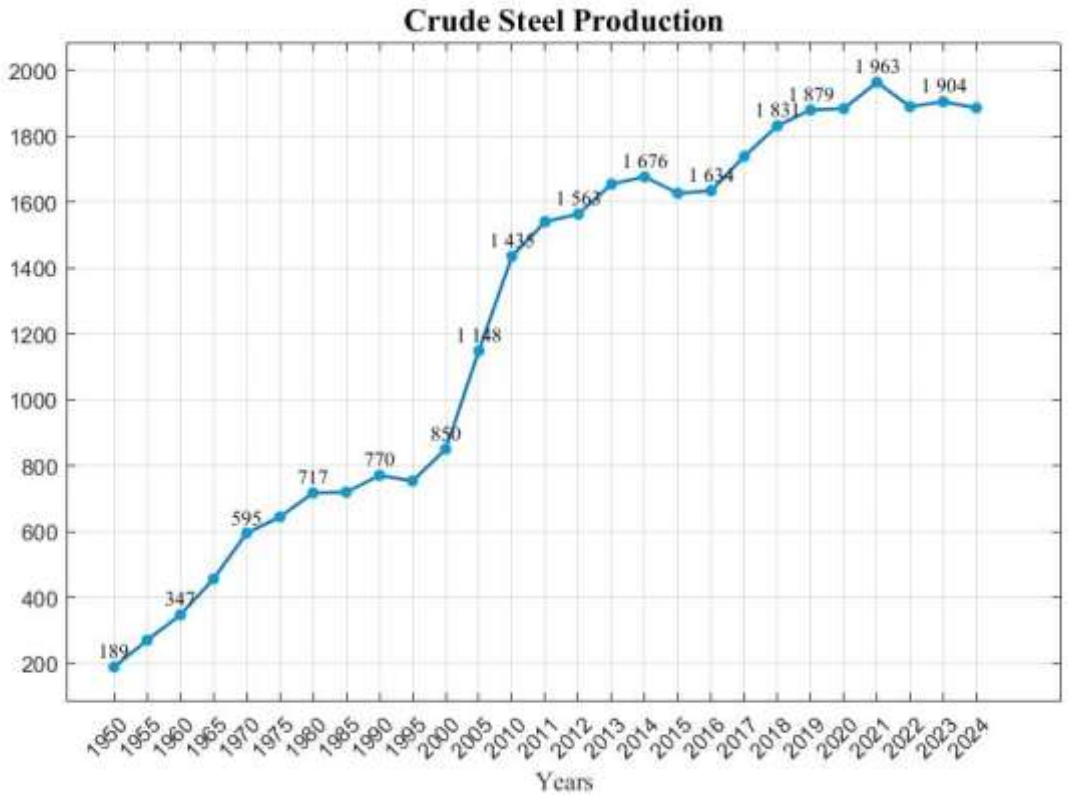

Figure 1-3. Crude steel production

As shown, world production has steadily increased from 189 Mt in 1950 to a record of 1963 Mt in 2021, according to data from World Steel Association [4]. However, after reaching this peak, a moderate decline can be observed, with a global decline of about 4,2% in 2022.

This decline can be attributed to multiple factors, but the main reasons are found in individual countries, especially the ones with larger share. In fact, China recorded a significant decrease in output, mainly due to the real estate crisis after 2021 [5]. Other major factors are related to the Europe: higher gas and electricity prices have increased production costs, decreasing of 3,5% in steel demand [6], and the war between Russia and Ukraine has almost interrupted the production of iron ore and steel, with a 70% decreasing in Ukraine steel production [7]. On the other hand, excluding China, the rest of the developing world growth of 3.5% in 2024, and India has emerged as strongest driver of steel demand growth since 2021, with its steel demand projected to increase by 8.0 % over 2024 - 2025 [5].

Generally speaking, steelmaking can be divided into two main pathways, differing in their main iron inputs. In primary steel production, which still represents the majority of global output (about 80 - 90%), the Blast Furnace - Basic Oxygen Furnace (BF - BOF) and the Direct Reduced

Iron - Electric Arc Furnace (DRI - EAF) routes are the dominant processes, while Smelting Reduction - Basic Oxygen Furnace (SR - BOF) route contribute for less than 1% to the global steel output. In these cases, the processes starts mainly from iron ore as the input raw material, which is first converted into iron (hot metal or DRI) and then refined into steel. In contrast, secondary steel production, which accounts for approximately 10 - 20% of global production, uses predominantly scrap as the main iron input and relies almost entirely on Electric Arc Furnaces (EAF).

Figure 1-4 schematically illustrates the two main steel production routes, distinguishing between primary and secondary production. The diagram is organized into three main stages: raw material preparation, where the inputs of the main processes are prepared (e.g. coke, sinter, and pellets); ironmaking, where iron is produced either in the Blast Furnace, DRI furnace, or Smelting Reduction furnace; and finally steelmaking, where the produced hot metal or DRI is refined into steel in Basic Oxygen Furnaces (BOF) or Electric Arc Furnaces (EAF).

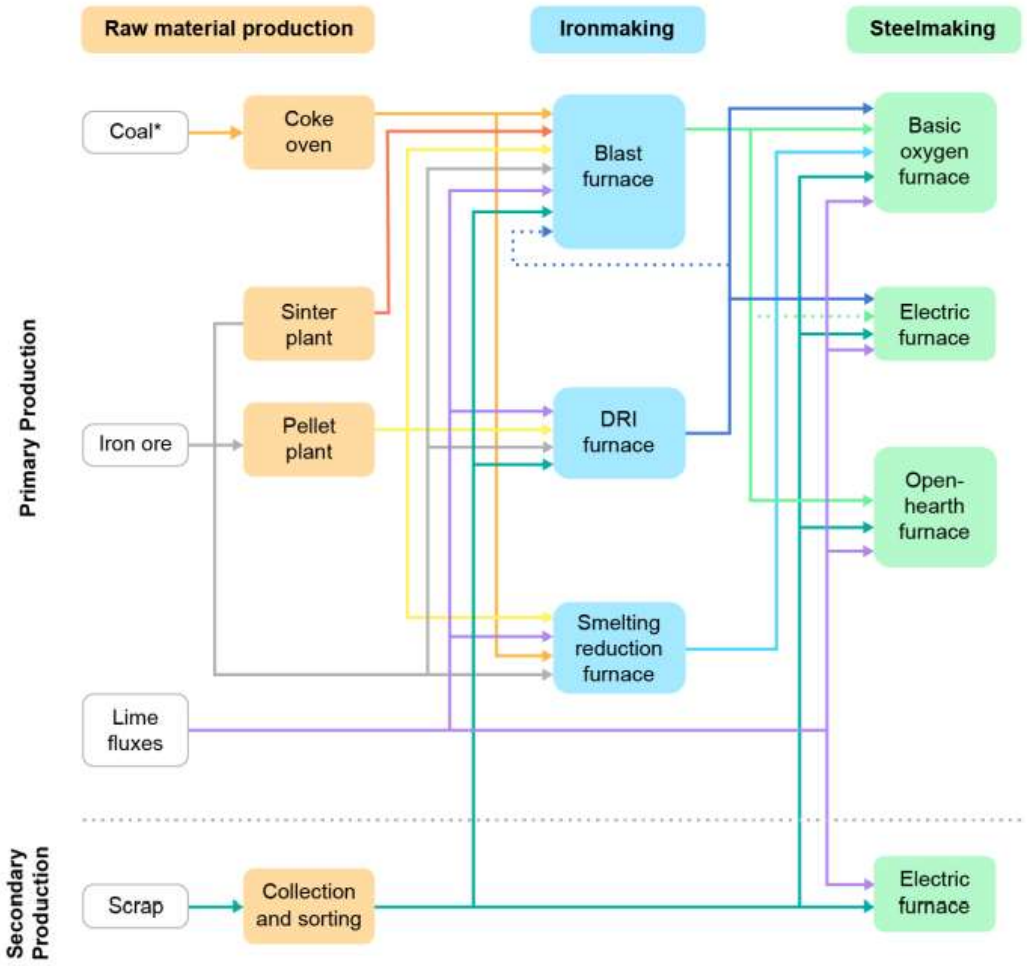

Figure 1-4. Main steel production pathways and material flows [2]

Both the primary and secondary route require large energy inputs. Energy provides heat to melt the iron input and to reduce the iron ore, removing oxygen atoms chemically.

Since scrap-based EAF bypasses the iron ore reduction stage, it results in the lowest specific energy use and CO_2 emissions among conventional steelmaking routes. However, ore-based primary routes still account for the vast majority of global crude steel production, so any deep decarbonisation strategy must primarily involve these primary routes.

A brief description of the main configuration follows, to clarify why these processes are energy and CO_2 intensive. Based on these reasonings, the section identifies ironmaking as an area with great level of decarbonization and motivates an assessment using natural gas based DRI as reference case.

1.1 BF – BOF Description

The Blast Furnace–Basic Oxygen Furnace process is the principal ore-based pathway for steelmaking, accounting for about 71,1% of global crude steel production [4]. It is a two-stage integrated process: iron ore is first reduced and smelted in the blast furnace, then the liquid metal produced, called hot metal or pig iron, is refined in the basic oxygen furnace. Figure 1-5 schematizes the overall route, from raw material preparation in dedicated sinter and pellet plants and coke ovens to crude steel production.

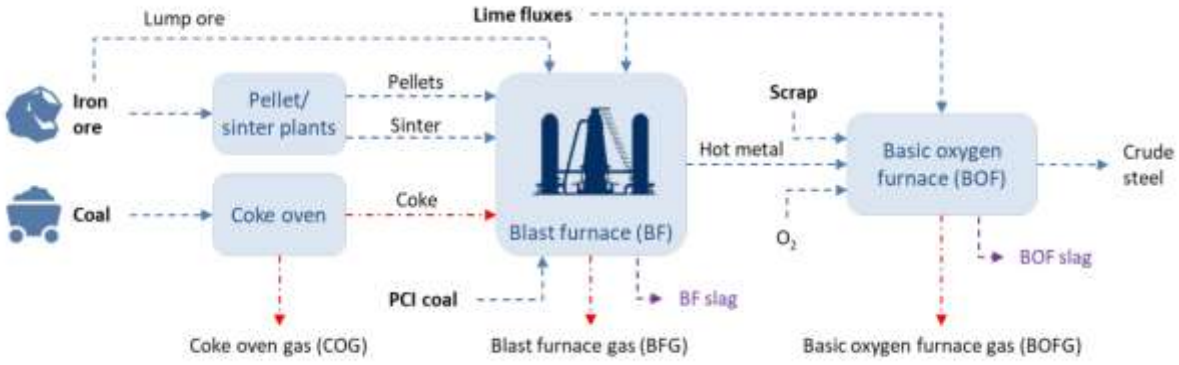

Figure 1-5. Basic Oxygen Steelmaking (BOS) pathway

In the blast furnace, a counter-current shaft reactor, iron ore is used as the iron-bearing raw materials, and coke and pulverised coal act as reducing agents and heat source. Additionally, lime and limestone act as fluxing agents to remove impurities, which are separated in the form of a liquid slag. Sinter, pellets and lump ore are charged into the upper part of a blast furnace together with coke and the lime fluxes, while pre-heated air (known as blast), enriched in oxygen, is blown into the furnace, injected through tuyeres from the bottom.

The hot blast reacts with the coke and coal forming carbon monoxide which rises through the furnace reducing the layers of iron ore to liquid metal and producing carbon dioxide as a by-product. The hot metal produced at the bottom contains about 4-5% of carbon and other impurities. The distribution of temperature inside the furnace can be around 200°C at the top of the vessel, while can exceed 1600°C at the bottom, and even 2000°C in the raceway zone [8]. Along with hot metal and slag, blast furnace operation generates a large flow of blast furnace gas, which is cleaned and recirculated as a fuel in hot-blast stoves, boilers and on-site power generation units [9].

Then, in the subsequent basic oxygen furnace step, the hot metal is charged together with a controlled amount of scrap and fluxes. Almost pure oxygen is blown into the molten metal: the exothermic oxidation reactions provide the heat needed to melt the scrap and lower the carbon content to the desired value, typically < 0.2wt%. Further, BOF gas and Slag are produced as by-products.

The process is highly energy intensive. In 2023 it required approximately 24 GJ per tonne of crude steel cast, strictly higher than the global average of about 21 GJ per tonne of crude steel cast [10]. Due to the extensive use of coke during the process, the carbon footprint is very high, amounting globally at 2.32 tonnes of CO_2 per tonne of steel cast in 2023 [10].

Despite its environmental impact, the BF-BOF technology remains the most attractive process because of its economies of scale: an individual blast furnace can produce up to 10,000 tonnes of hot metal per day, and integrated steel plants often exceed 5 million tonnes of steel output per year. This makes the process efficient and reliable from and industrial point of view, though very challenging to decarbonise.

1.2 DRI – EAF Description

The Direct Reduced Iron-Electric Arc Furnace route combines a shaft furnace for ironmaking process with an electic arc furnace for steelmaking, and represents the main ore-based alternative to the conventional BF-BOF process.

Direct reduction is defined as any process in which metallic iron is produced by the reduction of iron ore at temperatures below the melting point, typically in the range of 800-1100°C. The ironmaking step takes place in a shaft furnace, where pellets and lump ore are reduced by a reducing gas, typically produced from natural gas. Aproximately 92% of the DRI production relies on syngas obtained by reforming of natural gas, while the remaing share uses syngas derived by gasification process of coal. The product of this process, called Direct Reduced Iron

(DRI), can be batch-charged or fed continuously into an electric arc furnace, together with scrap and lime fluxes, to produce liquid steel with the required physical and chemical properties for casting. In practice, the EAF can be fed from almost 100% scrap up to high DRI percentage, providing flexibility in terms of raw material mix.

An example of DRI-EAF process is reported in Figure 1-6.

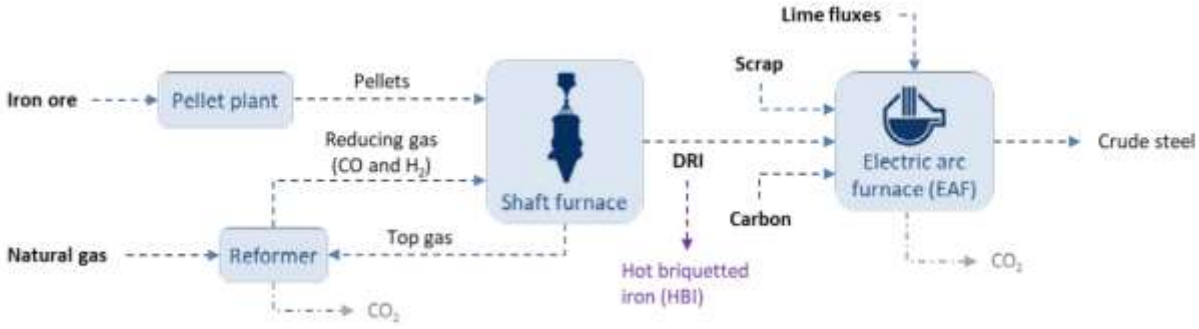

Figure 1-6. Natural gas-based direct reduced iron (DRI) to electric arc furnace (EAF) pathway

The two leading shaft furnace DRI processes are the MIDREX process and the Energiron/HYL ZR (Zero Reformer) process. For most sites employing gas-based DR furnaces, natural gas is the primary feedstock and is converted to reducing gas (carbon monoxide and hydrogen) either in an external reformer (as in the MIDREX process) or by in situ reforming (as in the Energiron/HYL ZR process).

DR plants can have high flexibility in the product output, being able to produce different types of DRI, depending on their handling, form or final use:

- Cold DRI (CDRI): cooled to about 50 °C in the lower part of the shaft furnace, then stored and used in a nearby EAF. It is often passivated to prevent reoxidation and loss of metallization.
- Hot DRI (HDRI): transported to an adjacent EAF at about 650°C, which allows recovery of sensible heat and reduces electricity consumption during melting.
- Hot Briquetted Iron (HBI): obtained by compacting porous DRI into dense briquettes, typically of 30×30×110 mm size and density > 5 g/cm³, which ensures safer handling, reduced reactivity, and suitability for the international market.

Further, the DRI product typically reaches a metallization rate between 90% and 96%. It also incorporates carbon from the reducing gas, resulting in carbon content ranging from 0,5% to 4%.

The use of DRI in EAF offers advantages compared with scrap only production. First, it reduces the dependence on the availability and quality scrap, which can be variable and contaminated with residual elements. Second, the controlled composition of DRI ensures more consistent chemistry in steelmaking, allowing better control of the final product properties. Nevertheless, achieving the required quality of DRI depends on the quality of iron ore pellet, or lump ore with low gangue content, which are more expensive and not always available.

From an energy point of view, the DRI-EAF path is less intensive than the BF-BOF route, but still requires a significant amount of both natural gas and electricity. According to the World Steel Association [10] the energy required by the process in 2023 was about 23 GJ per tonne of crude steel cast, slightly lower than the BF-BOF process. From a carbon footprint perspective, since emissions strongly depend on the type of reducing agent due to carbon intensity, natural gas based DRI-EAF releases around 1.43 tonnes of CO_2 per tonne of crude steel, which is considerably lower than the BF-BOF benchmark, almost 40% less.

Further, considering HDRI product directly charged in an EAF could result in energy savings of around 100-150 kWh per tonne of liquid steel.

The annual global DRI production in 2024 reached a record with 140.8 million tonnes, surpassing the previous value of 135.7 million tonnes in 2023 and confirming the constant annual growth trend observed since 2019.

Geographically the production is concentrated in a few keys countries: India is by far the largest producer with 54.7 million tonnes, followed by Iran with 34.1 million tonnes. Other important producers include Russia, Saudi Arabia, and Egypt, with an output of around 6–8 million tonnes each.

Overall, the DRI-EAF route represents a relatively small share of global steelmaking, accounting for 7-8% of the global steel output [11].

1.3 SCRAP – EAF Description

The steelmaking based on recycled steel scrap melted in an Electric Arc Furace, without the need of a reduction step as in the BF-BOF or DRI-EAF route, is usually referred to as a secondary steel production, since it does not use iron ore or other primary raw material, but instead it relies on remelting of existing metallic resources. Figure 1-7 provides a drawing of a Scrap-EAF process.

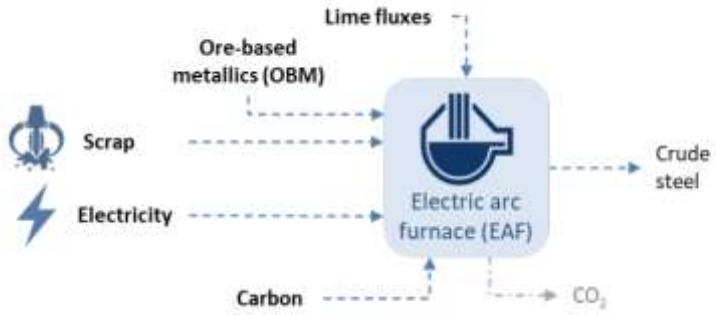

Figure 1-7. Scrap-based EAF or secondary steel pathway

Firstly the furnace is charged with metallic scrap, often complemented by a portion of DRI or HBI to control the chemistry of the final product. Then, a high voltage electric current generates the electric arc between the graphite electrodes and the metal, dramaticaly increasing the temperature and allowing the metallic charge to melt.

Globally the EAF crude steel production by route accounts for about 29%, considering both the primary and secondary production [4]. However this share is not equally spread on the countries. The leader on EAF steelmaking is United States, with more than 70% of crude steel production through this route, reflecting the abundance of steel scrap and lower electricity costs [12]. European Union follows, with around 40% of share, while in China the steelmaking is still dominated by BF-BOF route, accounting for 9-10% of EAF share [13][14].

From an energy perspective, the scrap-EAF route is the most efficient among conventional steelmaking process, requiring around 2.1 GJ per tonne of crude steel in final energy terms in 2023 [2], which corresponds to about 10 GJ when reported as primary energy in the World Steel Association [10]. This is less than half the energy demand of the BF-BOF parthway. The carbon footprint is also considerably reduced, at about 0.04 tonnes of direct CO_2 emissions per tonne of crude steel, and 0.34 tonnes of CO_2 per tonne of crude steel when including direct and indirect.

Nevertheless, this process faces some important limitation for growth of the production. First, because of the quality of metallic scrap, in particular contamination of other metal, such as copper or zinc, the final product by scrap-EAF can not be used for sectors that require high quality steel. Rather this steelmaking route is better suited to application in the construction sector [15]. In addition, although globally the recycled steel cover about 40-50% of the steel production, the global demand of steel is growing faster than scrap availability [16], and this "scrap gap" limits the expansion of scrap-EAF route in short terms.

Therefore, although scrap-EAF is crucial to lower average emissions, its expansion is constrained by scrap availability and quality.

1.4 Comparative Assesment

The three main steelmaking routes BF-BOF, DRI-EAF, and scrap-EAF show very different characteristics in terms of energy requirements, carbon footprint, and technical limitations. Table 1-1 provides a comparative overview based on the most recent data reported by IEA [2].

	Production [%]	**Energy Intensity [GJ/t_{cs}]**	**Direct CO_2 Emissions [t_{CO_2}/t_{cs}]**	**Total CO_2 Emissions [t_{CO_2}/t_{cs}]**
BF-BOF	71,1	21,4	1,20	2,20
DRI-EAF	7,2	17,1	1,00	1,40
Scrap-EAF	21,4	2,1	0,04	0,34

Table 1-1. Global production share, energy intensity and CO_2 emissions of the main steelmaking routes

Due to the central role of carbon as both fuel and chemical reductant in conventional steelmaking, the iron and steel sector accounts for roughly one quarter of global industrial CO_2 emissions and about 7% of total energy-sector emissions [2].

The BF-BOF route with coal injection directly emits around 1.2 t_{CO_2}/t_{cs}. In addition, it results in an average of 1.0 t_{CO_2}/t_{cs} in indirect emissions from electricity and imported heat generation. About 90% of BF-BOF production relies on coal injection, with the remaining share relying on injection of other fuels such as gas or charcoal, which results in a somewhat lower direct emission intensity. The considerable indirect emissions from the BF-BOF route result in part from use of steel off-gases for a large proportion of heat and electricity, and also from imported generation, which generally takes place on site, and also from imported electricity and heat [2].

DRI-EAF can achieve somewhat lower emission intensities. This is largely due to 70% of DRI-EAF production relying on natural gas rather than coal. A tonne of crude steel produced by natural gas-based DRI-EAF results in 1.0 t_{CO_2}/t_{cs} in direct emissions. At the current global average CO_2 intensity of electricity generation the route results in 0.4 t_{CO_2}/t_{cs} in indirect emissions from electricity generation.

The coal-based DRI-EAF route produces almost three times more direct emissions and a similar quantity of indirect emissions as its gas-based DRI-EAF counterpart.

Conversely, scrap-based EAF production relies primarily on electricity and has a much lower emission intensity. The route results in only about 0.04 t_{CO_2}/t_{cs} on a direct emissions basis, and 0.3 t_{CO_2}/t_{cs} in indirect emissions. In this case, direct emissions from the furnace itself are limited

compared to the other routes, and the overall indirect emissions are determined by the CO_2 intensity of the electricity mix used for the EAF.

Besides CO_2 emissions, it is important to highlight the production share and energy intensity of the three routes. The BF-BOF still dominates global steel production, accounting about 71,1% of output, while scrap-EAF and DRI-EAF follows with 21,4% and 7,2% respectively. From an energy perspective, BF-BOF is the most intensive route, with an average energy use of about 21.4 GJ/t_{cs}, while gas-based DRI–EAF reduces this requirement to around 17.1 GJ/t_{cs}. Scrap-based EAF shows the lowest energy intensity, about 2.1 GJ/t_{cs}, significantly lower than ore-based routes, reflecting the fact that it avoids the energy-demanding reduction of iron ore and relies mainly on remelting existing steel scrap.

Overall, the comparison in Table 1-1 shows that the BF - BOF route combines the highest CO_2 intensity with the largest share of global crude steel production, making it the main driver of sectoral emissions. Natural-gas-based DRI - EAF offers substantially lower emissions and slightly lower energy use, but still accounts for a relatively small fraction of global output, while scrap-based EAF achieves the lowest energy and CO_2 intensities yet remains structurally constrained by scrap availability and quality. These contrasting features imply that deep decarbonisation of the steel sector will require both maximising the use of scrap-based EAF and transforming ore-based routes; the role of DRI configurations in this context is discussed in the next section.

1.5 Decarbonization Perspective and Scope of the Present Work

From a future perspective, the steel industry will require a deep and consistent technological transformation in order to meet the global climate objectives and temperature goals established by the Paris Agreement. In Sustainable Development Scenario, the International Energy Agency [2] depicts an important reduction of direct CO_2 emissions, decreasing by 54% between 2019 and 2050, and by nearly 90% by 2070, while production level continues to grow moderately.

In this long-term scenario, considering the main routes of steelmaking, the BF-BOF pathway will continue to be predominant in crude steel production, and its decarbonisation will be a combination of two factors: the partial substitution of the coke with natural gas, that is less carbon intensive, or green hydrogen for reduction reaction, and a section dedicated to a separation and storage of CO_2 from the flue gases (CCUS). Then the DRI-EAF pathway is expected to gain increasing importance and reach significant results. Its flexibility can allow a

almost complete sustitution of natural gas input with hydrogen as the main reducing agent, helping in a deep emissions cut. Initiatives and projects such as HYBRIT in Sweeden, H2 Green Steel, or ArcerolMittal Hamburg are already demonstrating the technical faseability of hydrogen based reduction, promoting this way for industrial scale application. Further the decarbonization of electricity sector, reaching around 95% by 2050, will reduce drastically the indirect emissions associated with EAF operation.

Among the different technologies for DRI production, the MIDREX process is most industrially mature and the one that holds the largest share worldwide confirmed with more than half of the global DRI production, accounting for 54,1% [17] against the other two main actors, HYL/Energiron and Rotary Kiln, respectivetly around 11% and 32%.

Its current reliance on natural gas makes the MIDREX process a representative case of the actual industry, while at the same time the possibility of hydrogen adaption and operation with high hydrogen shares shows the possible future contributing to decarbonise the steelmaking industry.

The scope of this work is to present a technical analysis and comparison of the natural-gas-based MIDREX process (reference case) and a hydrogen-based DRI (H_2-DRI) configuration integrated with a high-temperature Solid Oxide Electrolyzer Cell (SOEC), calculating performance for both configuration and focusing on energy consumption and CO_2 emissions. The H_2-DRI system makes use of a mixture rich in hydrogen as reducing gas, and includes a small methane injection in the bottom part of the furnace, for iron carburization, to increase the carbon content of DRI and improve its quality for a downstream EAF unit. Further both cycle produce hot DRI (HDRI) with a discharge temperature of 650 °C. The block diagrams of the two plants are presented in Figure1-8.

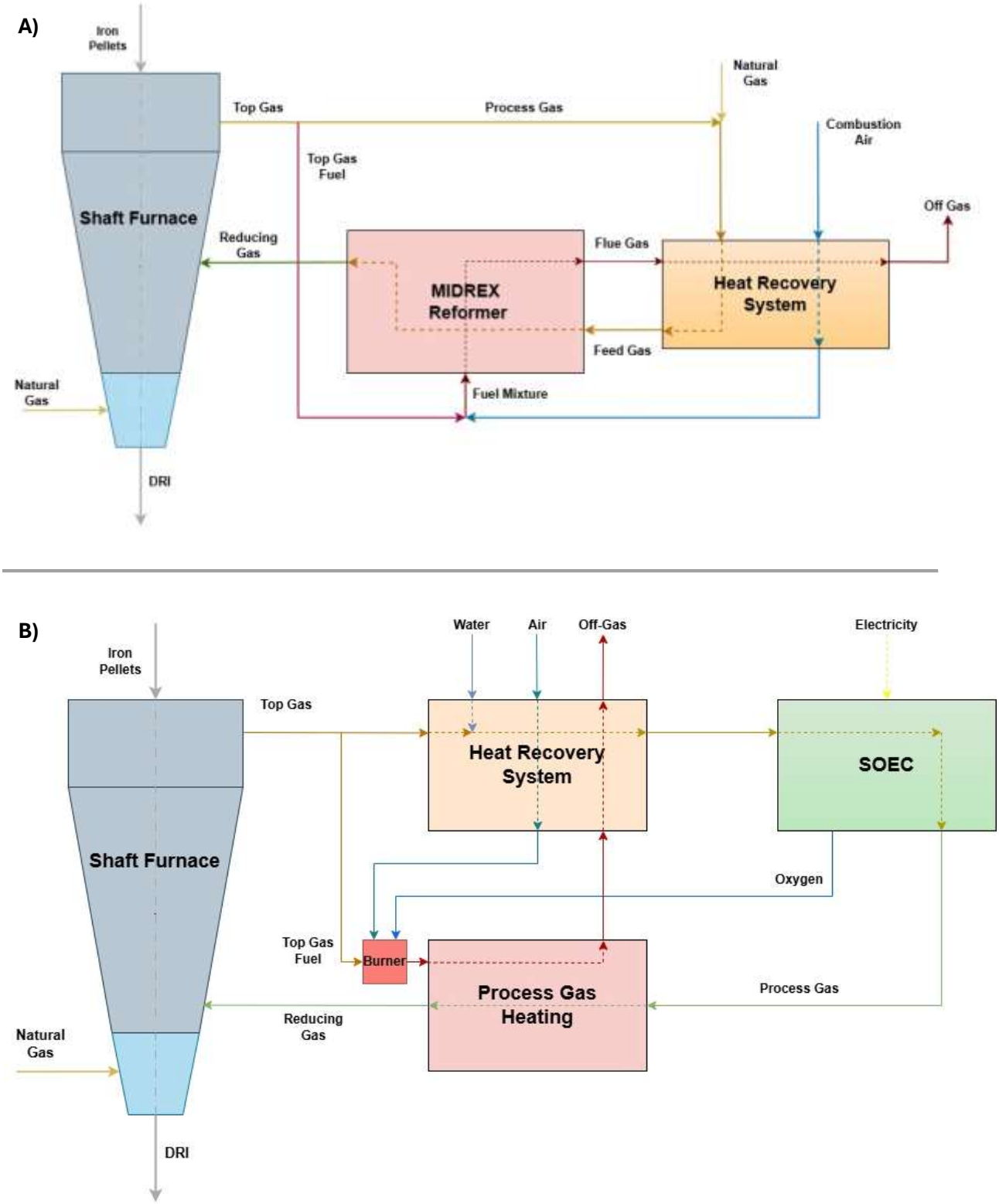

Figure 1-8. Block diagram DRI processes: Natural gas based MIDREX-DRI process (A) - Hydrogen based DRI proecess (B)

In the Midrex case (configuration A) the reducing mixture is prepared by the Midrex Reformer, fed by a mixture of top gas and natural gas; the thermal inuput is given by the Reformer burners, fueled with a fraction of top gas and pre-heated air.

In the H_2-DRI case (configuration B) the SOEC is fed by hot top-gas mixed with steam, both preheated to SOEC operating temperature, and a dedicated adiabatic burner supplies the thermal input by exploiting oxygen generated by the SOEC, together with small fraction of top gas and pre-heated air, providing the heat required for process gas preheat, SOEC feed preheat, combustion air and water make-up.

After building the two models with the software Aspen Plus and validating with literature data, the study reports the key results, showing gas and solid composition along the furnace, temperature trends, specific consumptions, and quantifies the effect of switching from reforming natural gas to electrolysis.

Then, beyond the technical comparison, an economic assessment follows under consistent operating conditions for the process (same shaft input temperature, bustle-gas RGQ, metallization etc.): capital costs are estimated from literature correlations and data available for the major sections, utilities are computed as operating costs, including electricity, natural gas, pellets, water etc. For a fair comparison, key performances indicator are compared referred to the tonne of DRI produced. In addition, a price of DRI and breakeven analysis are calculated to determine when the SOEC configuration becomes competitive versus the natural gas route; a sensitivity analysis explores the impact of the electricity and gas price and carbon cost.

In this work, the assessment is focused only on the DRI section: EAF is not included in the evaluation. Furthermore, the models of several systems are simplified and simulated as lump and steady-state models.

In summary this study is based on a like-for-like comparison between the natural-gas MIDREX route and the SOEC integrated H_2-DRI configuration. Recognizing that the SOEC are not yet a fully mature technology, the analysis quantifies the potential benefits and drawbacks of the adoption, lower NG use and CO_2 intensity versus higher electricity demand and added heat recovery complexity, and identifies the operating and market conditions under which the H_2 route can become a competitive and robust alternative in a decarbonizing perspective.

2 Processes Description

In this chapter, the two process configurations compared in this work are described: the reference natural-gas-based MIDREX process and the alternative H_2-DRI process with SOEC. For each configuration, the overall process flow diagram is presented and the main process units and streams are briefly described. The main sections, where the main chemical transformations take place, are then discussed in more detail in dedicated subsections: the reformer and the shaft furnace for the MIDREX layout, and the SOEC unit, together with some considerations on shaft furnace, for the hydrogen based layout.

2.1 MIDREX Process

The Midrex process is globally the most used gas based DRI technology, in which iron ore, in the form of pellets or lump ore, is reduced and converted into metallic iron. Two are the main cores of the process linked between them in a closed loop cycle. The first one is the Midrex reformer in which reducing gas is prepared, obtained by the reforming of the natural gas into a syngas rich in hydrogen and carbon monoxide; the second one is the Shaft Furnace, where reduction reactions between the iron oxides and reducing agents take place in order to produce the reduced metallic iron.

In Figure 2-1, the process scheme of the conventional Midrex natural gas based process is illustrated, highlighting four main sections: Shaft furnace, Topgas scrubber and compressor, Reformer and Hear recovery system.

In this process, the main components, Shaft Furnace and Reformer are modeled using the data available from literature and plant data available from Midrex reports [19] [20].

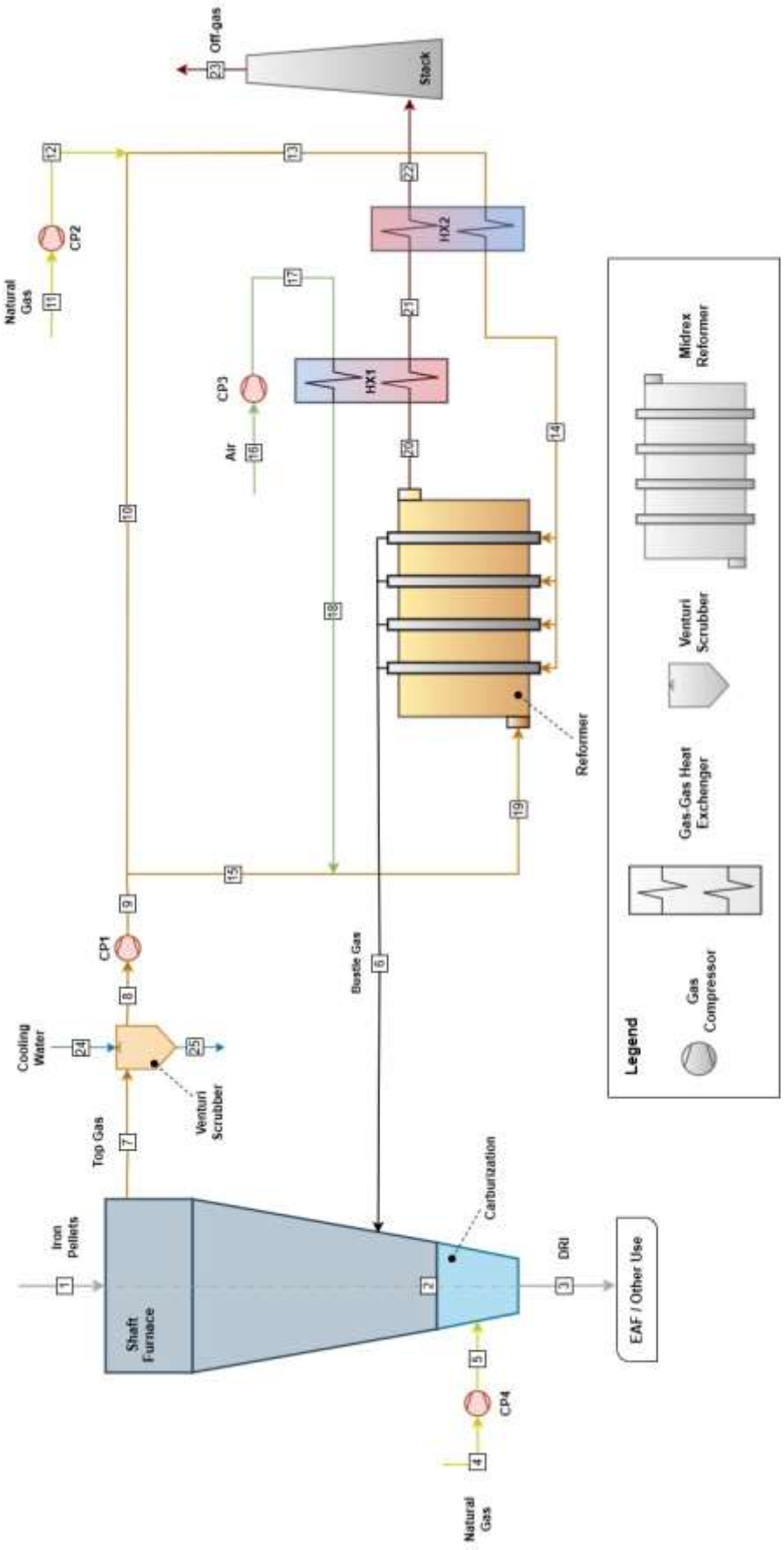

Figure 2-1. Process flow diagram of the NG-based MIDREX process

The iron pellets (stream #1 in Fig.2-1) enter at the top of the shaft furnace, operating at low pressure, slightly above ambient pressure, and descend by gravity through the reducing section of the reactor. At the bottom the reducing gas mixture, called Bustle Gas (#6), mainly containing Hydrogen (H_2), Carbon Monoxide (CO), Carbon Dioxide (CO_2) and water vapor (H_2O), enters the transition section of the furnace at about 980°C, flowing up and progressively removing oxygen from the pellets according to the reduction reactions, described in the following paragraph. Indeed, under the effect of the high temperature of the bustle gas, the iron pellets, based on Hematite (Fe_2O_3) are reduced to metallic iron (Fe), passing through Magnetite (Fe_3O_4) and Wüstite (FeO). The lower cone region of the furnace, below the bustle gas level, is characterized by an injection of natural gas (#4), which reacts with the reduced iron (#2) to produce Cementite (Fe_3C) and hydrogen, according to the iron carburization reaction with methane, increasing the carbon content of the product. In this configuration no cooling section is included and hot DRI is discharged to about 650°C (#3). The gas exiting at the top of the shaft furnace, called Top Gas (#7), is sent to the top gas scrubber, typically a Venturi Scrubber [21]: dusts and particulate matter carried by top gas form the furnace are removed and the strem is cooled down to about 50°C, condensing part of the water (#25) and consequently increasing the mole fraction of hydrogen and carbon monoxide in the gas mixture. The remaining stream (#8) is compressed to overcome the pressure drop of the system, and partially split into two streams. The majority (#10), about two thirds of the top gas stream [48], is mixed with natural gas make-up stream (#11), and after passing through the heat recovery section, is sent to the reformer as the Feed Gas (#14) at about 580°C. The remaining fraction, the Fuel Gas (#15), is mixed with combustion air (#16), appropriately pre-heated in the heat recovery section, and sent to the burners of the reformer, providing the heat required by the reforming reactions. Flue gases (#20) release heat in the heat recovery section, increasing the temperature of the feed gas and the combustion air, and off-gases (#23) leave the stack at the 150-250 °C [22]. Subsequentely, the reformed gas (i.e. Bustle Gas) re-enters the shaft furnace in the transition zone, closing the gas loop of the Midrex process.

To better understand the operation of the Midrex process, a detailed technical description of main the sections where the chemical reactions occur is provided: the external MIDREX reformer and the shaft furnace.

2.1.1 MIDREX Reformer

Midrex Reformer is the technological core of the process, as it produces the reducing gas for the shaft furnace. It consists of several hundred nickel catalyst-filled tubes [23] placed in a combustion chamber, where the fluxes, both inside (feed gas) and outside (flue gas) the tubes, move in co-current direction. The reformer is designed for up-flow operation, in order to facilitates a more uniform temperature profile along the tubes, and ensure stable catalyst performance. Preheated feed gas is distributed to the reformer tubes from the bottom, and hot reformed gas exits from the above and is collected in parallel duct on longitudinal axis of the reformer. In the combustion chamber both the main burners and auxiliary burners are designed to operate near stoichiometric combustion with about 1-2% oxygen in the flue gases [24].

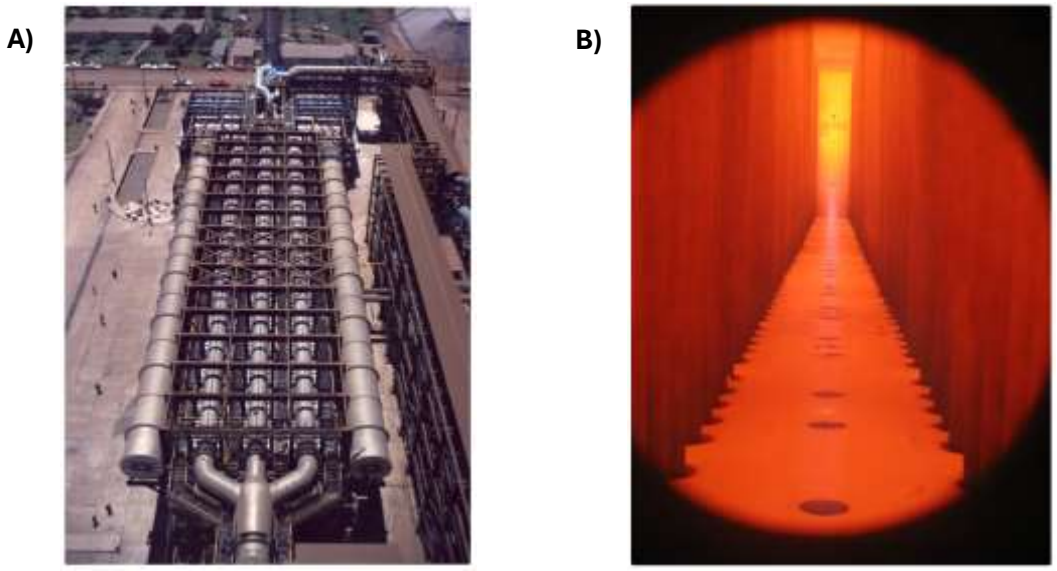

Figure 2-2. External (A) and internal (B) view of the MIDREX reformer [24]

The feed gas of the reformer consists mainly of the top gas, that is the gas exiting the shaft furnace, mixed with fresh natural gas as an external input for the reformer charge. Combustion chamber is fed with a stream obtained by combining combustion air, preheated to a designed temperature in a recuperator, with a split fraction of the top gas, typically about one third of the total flow. This configuration is possible mainly for two reasons: the volume expansion associated with the reforming reactions, and the presence of unreacted hydrogen and carbon monoxide in the top gas.

Finally, flue gas exiting the reformer is used to preheat both the main combustion fuel, to around 675°C, and the feed gas stream, typically to the temperature of 580°C. This heat recovery system provides an increase in reformer capacity and a reduction in the net plant energy consumption.

Since the feed gas contains an amount of carbon dioxide that is not negligible, due to the recycling of the top gas from the shaft furnace, the reforming process is not completely the conventional steam methane reforming but also involves significant dry reforming reactions. In particular the main reactions that occurs in the reformer are:

$$CH_4 + CO_2 \rightleftharpoons 2CO + 2H_2 \qquad \Delta H^0_{25°C} = +247\ kJ/mol \tag{2-1}$$

$$CH_4 + H_2O \rightleftharpoons CO + 3H_2 \qquad \Delta H^0_{25°C} = +206{,}0\ kJ/mol \tag{2-2}$$

$$CO + H_2O \rightleftharpoons CO_2 + H_2 \qquad \Delta H^0_{25°C} = -41{,}1\ kJ/mol \tag{2-3}$$

The reactions 2-1 and 2-2 are respectively the Dry Reforming (DR) and the Steam Methane Reforming (SMR), while the 2-3 is the Water Gas Shift (WGS).

Since both DR and SMR are strongly endothermic, the reformer requires high operating temperatures, typically in the range of 850-1000 °C, to shift the equilibrium towards the products. The WGS reaction, although slightly exothermic, takes place to adjust the H_2/CO ratio, which is maintained at around 1,5. The heat required by the endothermic reactions is supplied by the combustion of the fuel gas in the burners of the reformer. A quantity of the fuel gas is made by a fraction of top gas that contains unreacted species: methane, hydrogen and carbon monoxide. When it is mixed with preheated air, the oxidation of that species provides the heat power needed to sustain the process and maintain the operative temperature in the catalyst tubes. Oxidation reactions, respectively of methane, hydrogen and carbon monoxide are the following:

$$CH_4 + 2O_2 \rightarrow CO_2 + 2H_2O \qquad \Delta H^0_{25°C} = -802\ kJ/mol \tag{2-4}$$

$$H_2 + \frac{1}{2}O_2 \rightarrow H_2O \qquad \Delta H^0_{25°C} = -242\ kJ/mol \tag{2-5}$$

$$CO + \frac{1}{2}O_2 \rightarrow CO_2 \qquad \Delta H^0_{25°C} = -283\ kJ/mol \tag{2-6}$$

Further Midrex reformer, compared to classical reformer, operates at relatively low pressure, in the range of 2-4 bar, since the shaft furnace does not require high pressures, and to ensure a higher conversion of the methane.

An important aspect to take into account is the carbon formation and deposition in the reformer, deactivating the catalyst. Indeed, streams with high carbon content involve higher risk of carbon deposition, but this alone is insufficient to determine carbon formation. Among the carbon deposition reactions, the most relevant ones are:

$$2CO \rightleftharpoons C_{(s)} + CO_2 \tag{2-7}$$

$$CO + H_2 \rightleftharpoons C_{(s)} + H_2O \tag{2-8}$$

Because of the reaction 2-8, the presence of hydrogen or carbon monoxide increases the carbon formation. However, water prevents its formation, while carbon dioxide does not affect much, since in principle it reacts to methane to produce carbon monoxide. Considering the equilibrium constant, defined by activity coefficients, Midrex has developed its simplified version, called "k-factor" [22], that take into account the molar fraction of the i-species in the gas mixture, x_i, and exclude the pressure terms:

$$k_{factor} = \frac{x_{CO}\, x_{H_2}}{x_{H_2O}} \tag{2-9}$$

Generally, through commercial experience and research, MIDREX plants have been able to operate with k-factors around 0.5, with theoretical maximum value being 0.74.

For conventional technology, reformer inlet operates in the region where carbon deposition is thermodynamically favored. This mode of operation requires fine control over the temperature and composition of the inlet gas to prevent carbon deposition from occurring. The catalyst undergoes a sulfur passivation process to decrease its activity at the tube inlet, where the carbon reactions are heavily favored due to the lower temperature. Lower activity allows the feed gas to remain out of equilibrium until the gas reaches temperatures high enough not to favor carbon deposition.

As illustrated in Figure 2-3, the dashed line represents the k-factor at which MIDREX reformer operates; carbon deposition is favored by equilibrium in the region at temperature <650 °C, which is typical temperature region of feed gas preheats. [22].

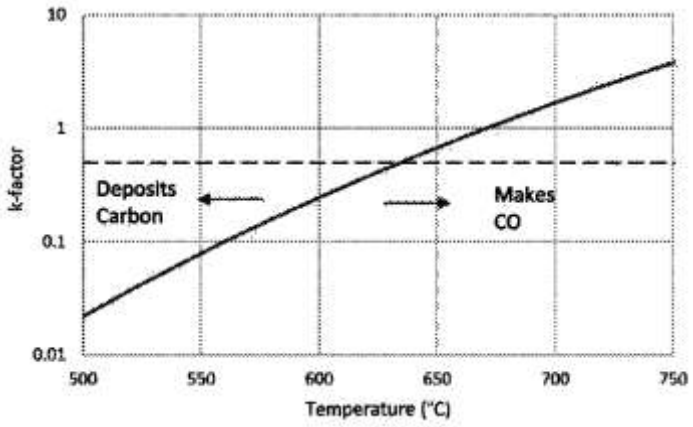

Figure 2-3. Carbon formation limits

With these operating condition, the Midrex reformer ensures a reformed gas composition rich in hydrogen and carbon monoxide, characterised by a specific Reformed Gas Quality (RGQ), defined as:

$$RGQ = \frac{x_{CO} + x_{H_2}}{x_{H_2O} + x_{CO_2}} \tag{2-10}$$

where the x_i represents the molar fraction of the i-species at the reformer outlet. This dimenesionless index expresses the excess of reducing agents with respect of the inert components in the gas. To ensure a complete reduction of iron oxides in the shaft furnace the RGQ is typically mantained above 9.5 [24].

In order to report the main operating parameters of the Midrex reformer, Table 2-1 summarise typical and key design values documented in reports and technical literature [24].

	UoM	**Inlet**	**Outlet**
CH	vol%	17	1
CO	vol%	19	35
CO_2	vol%	15	2
H_2	vol%	35	55
H_2O	vol%	13	6
N_2	vol%	1	1
Temperature	°C	580	980
RGQ	-	-	> 9.5
H_2/CO	-	-	1.5 – 1.7

Table 2-1. Typical MIDREX reformer inlet/outlet values

2.1.2 Shaft Furnace

The MIDREX shaft furnace is the core reactor of the MIDREX process, in which iron ore pellets and lump ore are reduced to DRI. Modern industrial shaft furnaces typically have a height of about 20 m and a diameter of 5-7 m, with the geometric size being one of the main parameters controlling production capacity [25] . Typically NG-based DRI plants present a single shaft furnaces with annual capacities between about 1.0 and 2.5 Mt of DRI per year [25]. The increasing capacity up to 3 Mt/y is actually under development [26]. This scale underlines that the MIDREX shaft furnace is already a full industrial reactor, comparable to a blast furnace in terms of volume output, while operating at significantly lower temperatures and with a different reduction mechanism.

The shaft operates as a vertical counter-current reactor charged with the iron ore pellets from the top and fed with hot reducing gas from the lower part; this configuration ensures the right heat and mass transfer for the required reactions and maximizes the utilization of the gas. Further this configuration also provides a stable and controlled operation, high productivity and uniformity of the final product.

Figure 2-4. Tosyali Algerie shaft furnace [27]

From an operational perspective, the furnace is typicallly divided mainly in three sections, the last depending on the type of DRI required. The upper-middle part is called “Reducing zone”, the middle part is “Transition zone”, while the lower part “Cooling zone” is used in case that the product desired product is cold DRI (CDRI).

In this present work the final part of the furnace, the cooling zone, is not described since hot DRI (HDRI) is considered as final product of the base case MIDREX plant.

In the reducing zone the progressive conversion of the iron ore takes place. In nature the iron ore is mainly based on his oxidised form, Hematite Fe_2O_3, with about 30.05% of oxygen content. The Hematite is reduced to metallic iron by three consequent chemical reactions, passing through the intermediate oxidized iron compounds, each with less content of oxygen. Firstly it is converted to Magnetite, Fe_3O_4, with an oxygen content approximately 27.64%, further reduced to Wüstite, FeO, containing about 22.27% oxygen. The final step of the sequence is the complete reduction removing theoretically the whole oxygen content, and obtaining metallic iron Fe.

This reduction sequence occurs thanks the chemical interacions with a gas having great affinity to the oxygen. hydrogen, H_2, and carbon monoxide, CO, are the typical reducing agents: while reducing iron ore, those chemical compounds are oxidised respectively to steam water, H_2O, and carbon dioxide, CO_2.

Reductions reactions carried out by Hydrogen over the iron ore pellets are as follows:

$$3Fe_2O_3 + H_2 \rightleftharpoons 2Fe_3O_4 + H_2O \qquad \Delta H^0_{25°C} = -11.715\ kJ/mol \qquad (2\text{-}11)$$

$$Fe_3O_4 + H_2 \rightleftharpoons 3FeO + H_2O \qquad \Delta H^0_{25°C} = +77.464\ kJ/mol \qquad (2\text{-}12)$$

$$FeO + H_2 \rightleftharpoons Fe + H_2O \qquad \Delta H^0_{25°C} = +23.873\ kJ/mol \qquad (2\text{-}13)$$

The overall reaction can be resumed in a single step:

$$Fe_2O_3 + 3H_2 \rightleftharpoons 2Fe + 3H_2O \qquad \Delta H^0_{25°C} = +95.484\ kJ/mol \qquad (2\text{-}14)$$

Considering the standard enthalpy of formation of this global reaction, it is possible to observe that the overall reduction of hematite in metallic iron with hydrogen is endothermic. As a consequence, this reaction require heat from the system in order to maintain an efficient reduction, and it contributes to lower down the temperature profile of the furnace.

Similarly, reduction reactions with carbon monoxide can be summarised as follows:

$$3Fe_2O_3 + CO \rightleftharpoons 2Fe_3O_4 + CO_2 \qquad \Delta H^0_{25°C} = -52.904\ kJ/mol \qquad (2\text{-}15)$$

$$Fe_3O_4 + CO \rightleftharpoons 3FeO + CO_2 \qquad \Delta H^0_{25°C} = +36.274\ kJ/mol \qquad (2\text{-}16)$$

$$FeO + CO \rightleftharpoons Fe + CO_2 \qquad \Delta H^0_{25°C} = -17.317\ kJ/mol \qquad (2\text{-}17)$$

Also in this case it is possible to describe the reduction of hematite into metallic iron in a single step:

$$Fe_2O_3 + 3CO \rightleftharpoons 2Fe + 3CO_2 \qquad \Delta H^0_{25°C} = -28.085\ kJ/mol \qquad (2\text{-}18)$$

As before, considering the standard enthalpy of formation, the global reaction is exothermic, releasing energy during its process. These reactions contributes to the reduction of the iron oxide and provide to release heat to the system, exploited then from endothermic reactions with hydrogen.

Due to the partial thermal compensation between the CO and H_2 reduction steps, the axial temperature profile of the furnace remains relatively smooth, with no pronounced excursions. A variation of the H_2/CO ratio could be significant in therms of temperature profile: increasing the H_2 fraction makes the overall reduction more endothermic, requiring a higher bustle-gas temperature, or a higher gas flow rate to maintain the target temperatures, while a higher CO concentration has the opposite effect and tends to increase the internal heat release.

Immediately below the reduction zone, after bustle gas distribution, in the Transition Zone, a controlled flow of natural gas is added into the furnace, with the purpose of adding and increasing the carbon content inside the metallic iron produced in the reducing zone. This natural gas injection promote the carburization reaction of the iron, integrating carbon in its structure as iron carbide (Fe_3C) and releasing hydrogen.

Considering methane as major component of the natural gas, the main reaction that occurs is:

$$3Fe + CH_4 \rightleftharpoons Fe_3C + 2H_2 \qquad \Delta H^0_{25°C} = +99{,}6\ kJ/mol \qquad (2\text{-}19)$$

These carbon-forming reactions are endothermic, so the double effect is to reduce the temperature of the final DRI product to typically 650°C, considering an HDRI discharge.

Percentages of carbon content inside the DRI are necessary due to its final use. In particular, using DRI in EAF allows to reduce any FeO unreacted to metallic iron. Any remaining carbon is available for oxidation and can be burned to provide additional heat energy supplementing the heat from the electric arc. Further using additional carbon helps to melt the steel quicker and increases productivity. However, it must be noted that excessive carbon in the DRI will be in the bath until it is blown down with oxygen. This extra time consumed in decarburizing causes a decrease in productivity of the EAF [28].

DRI can have around 0.5 - 4 wt% carbon depending on the process, the type of reducing gas, quality of the iron ore pellets and the way in which DR plant is operated. Most EAF steelmakers prefer to use DRI with 1.5 - 3 wt% carbon, but the optimum carbon level varies based on metallic charge mix and the steel grade produced [21].

Further, the carbon content inside the DRI can affect also the average density of the product. In this regard, the trend is shown in Figure 2-5, in which the increase of the carbon content causes a significant decreae in the final product density.

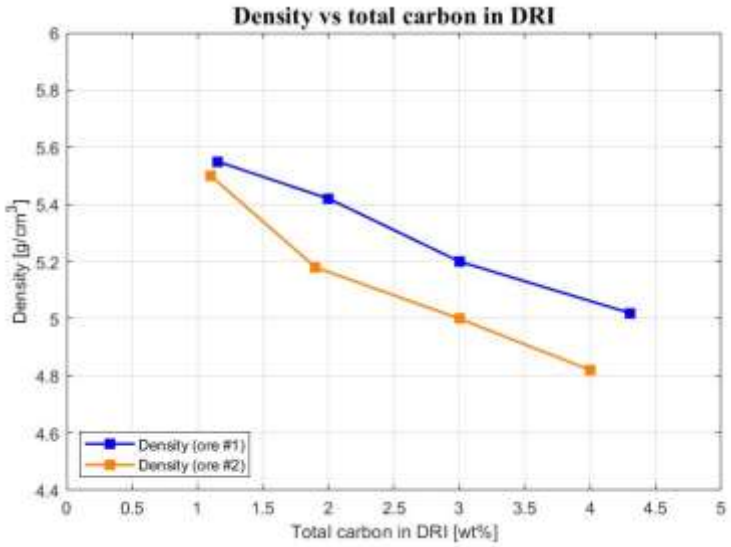

Figure 2-5. Density variation with carbon content in DRI [29]

At the shaft furnace solid outlet, the product quality is commonly expressed by the degree of metallized iron, that is called metallization, defined as the fraction of iron presented as metallic iron with respect at the total iron in the DRI:

$$M_{\%} = \frac{Fe^0}{Fe_T} \times 100 \qquad (2\text{-}20)$$

where M is the percent of metalization, Fe^0 is metallic iron with iron carbide included, and Fe_T is the total iron in DRI including metallic iron, iron carbide and the remaining iron as oxide (FeO). Products with metallization lower than 90% are called pre-reduced material or Remet, whereas those with metallization higher than 90% are classified as DRI. Pre reduced material are typically produced during the start up or shut down steps; this material is recycled back in small and controlled percentages to reactor [30].

At the shaft furnace top outlet the reducing gases, exit with a typical concentration of 33-49 mol% for H_2, and 19-26 mol% for CO; after a pre heating iron ore section, the temperature of the top gas leaving the shaft furnace ranges from 350-400 °C [31].

About operative pressure, Midrex shaft furnace operates at a relatively low pressure (≤ 1 barg), which simplifies the charging and discharging systems [32].

2.2 H_2 – DRI with SOEC

The second configuration investigated, adopts an innovative DRI production pathway, that eliminates the natural gas as reducing agent. The reducing gas is generated electrochemically by a Solid Oxide Electrolyzer Cell (SOEC), which produces hydrogen from steam, or hydrogen and carbon monoxide from steam and carbon dioxide via co-electrolisis. In this way, the conventional natural-gas reformer and its associated fuel consumption are replaced by a high temperature electrolysis unit supplied with electricity. The process remains a close loop with a top gas recycle, while the heat recovery system is reconfigured in order to provide the duty and temperature to each streams. Finally the primary input of the cycle shifts from natural gas to water.

Figure 2-6 depicts the process scheme, highlighting the main sections of the cycle as shaft furnace, SOEC, filter and scrubber, compressors and heat recovery system, and the main streams, each with its own number.

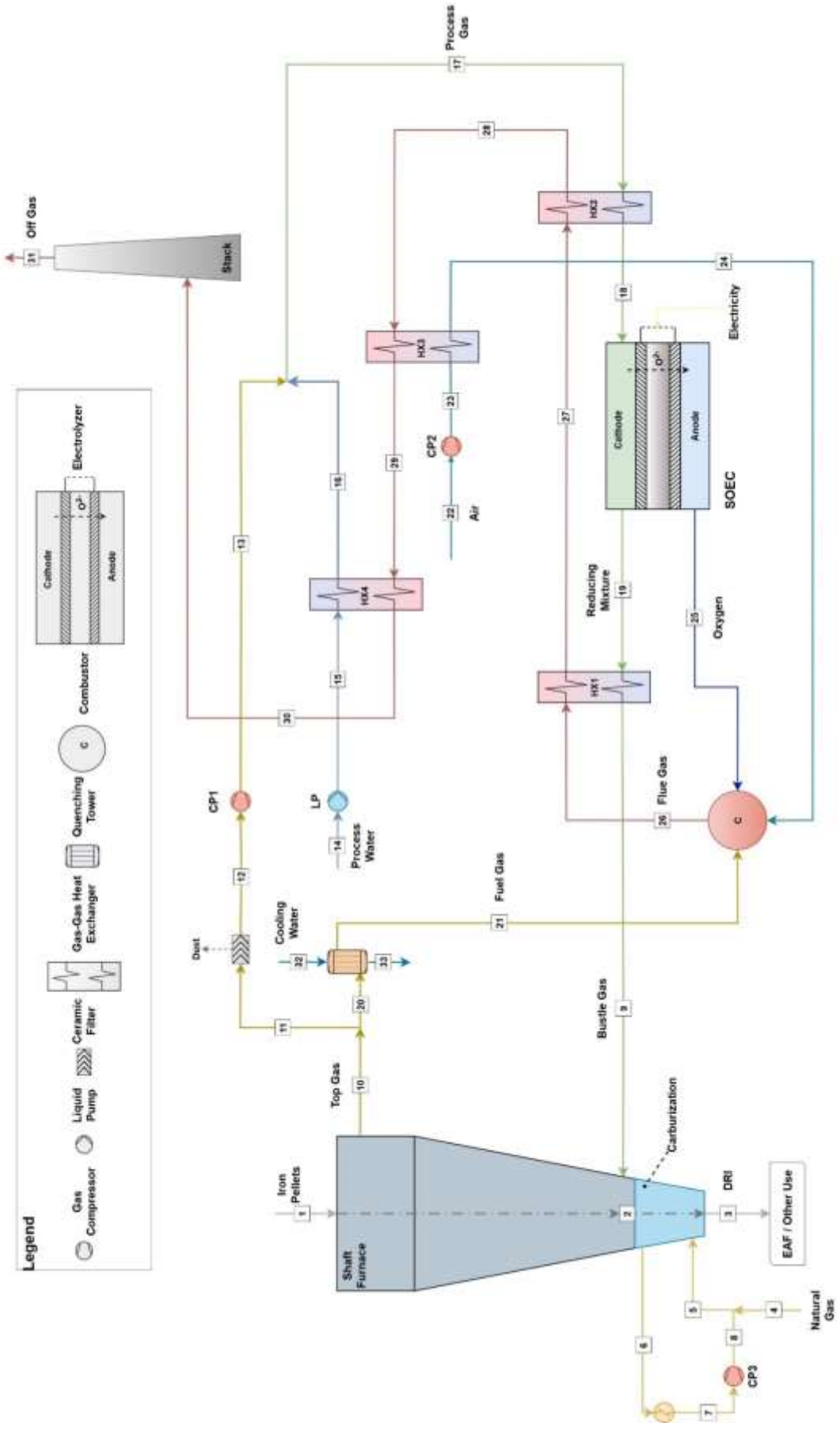

Figure 2-6. Process flow diagram of the H_2-DRI process with SOEC

In this configuration, the top gas leaving the shaft furnace (stream #10) is split into two streams as the base case: the major fraction is recycled in the loop as process gas, while a smaller part is sent to the burner (#20) to prepare the combustion mixture. The majority of the stream (#11) is cleaned through the ceramic filter and compressed to overcome the pressure drop of the reducing gas circuit, then it is mixed with steam (#16) coming from process water (#14), appropriately heated up in HX3. The mixture called process gas (#17) is preheated at the operative temperature for the electrolysis about 700 °C (#18), and sent to the cathode side of the high temperature electrolyser based on SOEC technology. The reducing mixture rich in hydrogen (#19) is heated up and enter the shaft furnace at the operative temperature to reduce iron oxides, at 980 °C (#9). The remain fraction of the top gas (#20) is cooled close to ambient temperature to remove water content and consequently increase the volumetric lower heating value of the mixture. It is mixed with air (#22), properly preheated, and pure oxygen (#25), recovered from the anode side of the electrolyser. These three streams feed the burner as fuel enriched in oxygen, then the exiting flue gases (#26) supply the heat recovery train for reduced gas exited from the SOEC, process gas, air and water, and leave the stack at 150-250 °C [22]. The shaft furnace operates as the base case, in which iron ore (#1) is charged from the top and leave the furnace as DRI in the bottom (#3). The only natural gas consumption (#4) is related to the carburization section in the lower part of the furnace. Since this is the only carbon input in the cycle, the final carbon content in the DRI product is lower compared to the reference case.

As the previous case, a detailed explanation of the most important components is provided in the next paragraphs, taking into account that about the furnace, few differences are highlighted.

2.2.1 Solid Oxide Electrolyzer Cell (SOEC)

A solid oxide electrolyzer cell (SOEC) is an electrochemical cell capable of converting steam (and/or carbon dioxide) to hydrogen (and/or carbon monoxide) and oxygen. The SOEC consists of a ceramic oxygen ionic conducting electrolyte, sorrounded by two porous electrodes, operating at high temperature, typically in the range 600-850°C. Considering for explanation only H_2O, steam is converted at the cathode into hydrogen and oxygen ions under the uptake of electrons. Under an applied voltage the oxygen ions are transported through the dense ceramic oxygen ion conducting electrolyte to the anode where oxygen is formed with the release of electrons. Figure 2-7 schematically depicts the SOEC device, with input and output streams. In this work air inlet is not considered.

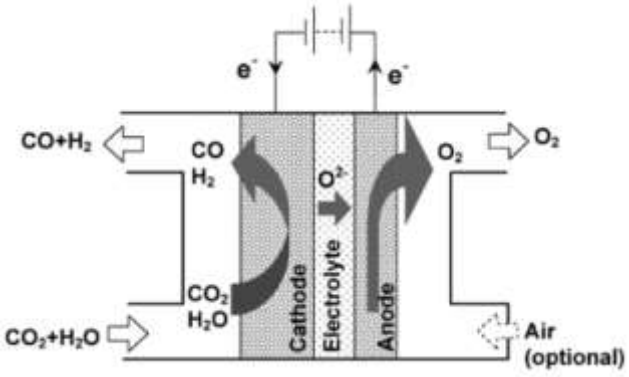

Figure 2-7. Schematic representation of a Solid Oxide Electrolyzer Cell for co-electrolysis of H_2O and CO_2

Considering only H_2O electrolisis for semplicity, the electrochemical reactions that take place in a SOEC can be summarized in a single step as:

$$H_2O \rightarrow H_2 + \frac{1}{2}O_2 \tag{2-21}$$

while the single reactions at cathode and anode side are the following:

cathode: $$H_2O + 2e^- \rightarrow H_{2(g)} + O^{2-} \tag{2-22}$$

anode: $$O^{2-} \rightarrow \frac{1}{2}O_{2(g)} + +2e^- \tag{2-23}$$

CO_2 proceeds through analogous elementary steps.

In general there are mainly two types of electrolyzers, depending on their operation temperature: low temperature electrolyzer (LTE) and high temperature electrolyzer (HTE).

LTE are devices that can achieve energy efficiencies about 67-74% on a LHV basis [33] : the major problem is the high electric energy consumption which can degrade the competitiveness of the process [34]. Although HTE is not mature technology, it presents a significant potential since the water electrolysis is strongly endothermic reaction.

The total energy demand from a electrolysis reaction, ΔH, is given by the sum of electric energy demand, ΔG, and heat demand, TΔS, represented by the relation:

$$\Delta H = \Delta G + T\Delta S \tag{2-24}$$

Considering an increase of temperature the heat term become greater, while the electric energy term decrease to maintain constant or slighty increasing the total energy demand. In Figure 2-8 it is depicted the thermodynamic of water electrolysis at a steam pressure of 1 bar.

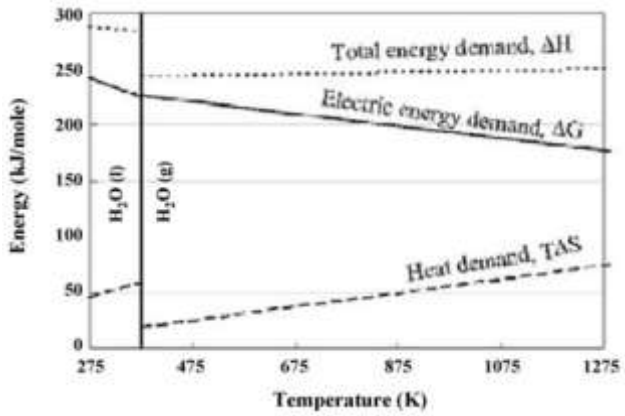

Figure 2-8. Total energy demand in function of temperature for water electrolysis [34]

Operating at higher temperature should mean a significant decrease in electric energy demand, and the heat demand could be supply by a heat recovery system in processes with high operative temperature.

In order to set the operative voltage of the SOEC cell, the reversible voltage E_{rev} and the thermoneutral voltage E_{tn} should be considered. E_{rev} represents the minimum theoretical potential set by Nernst Equation, while the E_{tn} defines the heat balance of the cell. The following equations represents respectivetly E_{rev} and E_{tn} :

$$E_{rev} = \frac{\Delta G}{nF} \tag{2-25}$$

$$E_{tn} = \frac{\Delta H}{nF} \tag{2-26}$$

where n is the number of electrons involved in the reaction and F is the Faraday's constant. Considering the thermoneutral voltage, three are the possible operating cases: when the voltage

cell, V_{cell} , is lower than E_{tn} it means that heat must be supplied to sustain the endothermic reactions; when it is greater heat needs to be dissipated; when the voltage cell is around the thermoneutral voltage the cell is in balance.

In practice the actual operating voltage is higher than E_{rev} because of activation, ohmic and concentration overpotentials.

E_{rev} and E_{tn} in water electrolysis at 25°C and 1 bar are respectively 1,23V and 1,48V (HHV basis, liquid water), while decrese to 1,00V and 1,29V at high temperature, around 700°C, LHV basis [35] [36].

In this present work the SOEC cells are set to operate close to thermoneutral voltage by pre-heating the inlet feed at the operative temperature of the device, around 700°C, so that no external heat input is required and only electricity is supplied to the stack. The electrical demand is computed from the oxygen production using the Faraday's Law and and an assumed cell voltage. The required current is given by:

$$I = 4Fn_{O_2} \tag{2-27}$$

while the stack DC power is given by

$$P_{DC} = V_{cell}I \tag{2-28}$$

The stack AC power is computed by assuming a DC/AC conversion of 0.95.

2.2.2 Shaft Furnace

The Shaft furnace has already been described in section 2.1.2 together with the reduction reactions 11-13 with hydrogen, and 15-17 with carbon monoxide. In this paragraph only the operational differences for this cycle configuration are highlighted.

As it is shown in the general description of this cycle, the SOEC prepares the reducing gas, and for this reason, iron oxide reduction is almost entirely based on the conversion with hydrogen. The overall reaction (Eq. 2-14) is endothermic, the heat release provided by the CO reactions is negligible. Maintaining the operative inlet temperature of the bustle gas constant, having only endothermic reactions means a possible outlet top gas temperature too low with respect to the typical temperature range. To avoid this issue, an excess of reducing gas is adopted; operating at a higher gas to solid ore ratio supplies additional sensible heat, sustaining and maintaining the target of the furnace temperature profile without raising the inlet temperature.

At the bottom of the furnace the carburization section remains the only use of natural gas; in this configuration the carbon content inside the DRI is roughly half of that in the base MIDREX case. In principle, increasing the natural gas flow for carburization would allow higher carbon levels in the DRI, but with the consequence of higher CO_2 emissions and operating costs due

to the additional fuel consumption. For these reasons, in the SOEC based configuration, a lower carbon content in the discharged DRI is accepted, and the implications for downstream operations are discussed in the following chapters.

3 Aspen Model/Validation/Results

This chapter describes the development and the validation of the Aspen Plus^{TM} model for the two plant configurations presented in Chapter 2, base case MIDREX with reformer and H_2-DRI route with SOEC.

Aspen Plus is a chemical process simulation software used by chemical and related industries to design, model, and optimise industrial processes. This software predicts process behaviour by solving engineering relationships, i.e. mass and energy balances, phase and chemical equilibrium calculations, and, where applicable, reaction kinetics, using thermophysical properties from selected property methods. Given reliable thermodynamic data, realistic operating conditions, and the rigorous equipment models, it is possible to simulate the modeled plant behavior and generate plant indicators and results.

This chapter has two main objectives: first, to translate literature assumptions into input data for the two process flowsheets; second, to validate the models by comparing simulation output with published reference data. Following validation, a critical discussion of the main differences between the base case MIDREX configuration and the H_2-DRI with SOEC alternative is presented.

3.1 Simulation Approach

The thermophysical properties of the gas phases streams are estimated using the GERG2008 equation of state (EoS), which is the 2008 extension of the GERG-2004 EoS model for the calculations of thermodynamic properties and phase equilibrium of natural gas, hydrogen, hydrocarbon mixtures. This is a highly accurate, wide-range equation of state that has been adopted as a international reference standard (ISO-20765) suitable for all natural gas applications. In this work, GERG2008 is applied to the reducing gas loop and the associated units block, covering the main species H_2, CO, CO_2, CH_4, H_2O. The complete 21 component of GERG model is listed in the references [37] [38] [39] [40].

Liquid water and steam, especially in the water make-up and units with phase change, are calculated with the IAPWS-95 property method. The IAPWS-95 formulation is in the form of a fundamental equation explicit in Helmholtz free energy and covers a validity range for temperatures from the melting line (lowest temperature 251.2 K at 209.9 MPa) to 1273 K and pressures up to 1000 MPa [41]. In this entire range of validity, it reproduces the most accurate

reference data within their experimental uncertainty, providing thermodynamically consistent properties of both liquid water and steam.

The thermodynamic properties of the solid components in the iron pellets and DRI produced are not accurately described by the database available in the software.

It is possible to overwrite the database parameters as function of temperature range and Aspen computes the thermodynamic properties of components using the Barin's equations, that are in order Gibbs free energy, enthalpy, entropy and heat capacity [42]:

$$G_i^{*,\alpha}(T) = a_{n,i}^{\alpha} + b_{n,i}^{\alpha}T + c_{n,i}^{\alpha}T\ln(T) + d_{n,i}^{\alpha}T^2 + e_{n,i}^{\alpha}T^3 + f_{n,i}^{\alpha}T^4 + g_{n,i}^{\alpha}T^{-1} + h_{n,i}^{\alpha}T^{-2} \quad (3\text{-}1)$$

$$H_i^{*,\alpha}(T) = a_{n,i}^{\alpha} - c_{n,i}^{\alpha}T + d_{n,i}^{\alpha}T^2 - 2e_{n,i}^{\alpha}T^3 - 3f_{n,i}^{\alpha}T^4 + 2g_{n,i}^{\alpha}T^{-1} + 3h_{n,i}^{\alpha}T^{-2} \quad (3\text{-}2)$$

$$S_i^{*,\alpha}(T) = -b_{n,i}^{\alpha} - c_{n,i}^{\alpha}(1 + T\ln(T)) - 2d_{n,i}^{\alpha}T - 3e_{n,i}^{\alpha}T^2 - 4f_{n,i}^{\alpha}T^3 + g_{n,i}^{\alpha}T^{-2} + 2h_{n,i}^{\alpha}T^{-3} \quad (3\text{-}3)$$

$$C_{p,i}^{*,\alpha}(T) = -c_{n,i}^{\alpha} - 2d_{n,i}^{\alpha}T - 6e_{n,i}^{\alpha}T^2 - 12f_{n,i}^{\alpha}T^3 - 2g_{n,i}^{\alpha}T^{-2} - 6h_{n,i}^{\alpha}T^{-3} \quad (3\text{-}4)$$

where α refers to an arbitrary phase which can be solid, liquid or ideal gas, the * identifies the pure components, standard state molar properties of the i-species. The Barin coefficient a-h are obtained in the specific range of temperature denoted by the n index.

The enthalpy of solid reduction reactions computed by the software using the Barin equation was compared against the NASA database in the temperature range of 298–1200 K. The resulting average error of about 1% across this range is considered consistent for the method validation.

3.2 Modeling Assumptions

This section introduces the overall Aspen Plus modeling strategy adopted for both the MIDREX cycle and the H_2-DRI configuration with SOEC. The aim is to reproduce consistently the main mass and energy flows of an industrial natural gas MIDREX plant, and to ensure a fair comparison between the two configurations by keeping the shaft furnace and plant capacity unchanged while modifying only the reducing gas generation.

Both models are developed as steady-state simulations. Each unit is represented by a zero dimensional block (0D), while the shaft furnace is modeled through a staged approach described in Sections 3.2.1-3.2.2, detailing the adopted inputs, assumptions, and Design Specifications

for each configuration, whereas the corresponding simulation results and their discussion are presented in Sections 3.3 - 3.5.

3.2.1 MIDREX Process Modeling

The Aspen Plus layout of the MIDREX cycle is presented in the following two figures. Figure 3-1 shows the shaft furnace section, while Figure 3-2 represents the reducing gas preparation through the reformer with the heat recovery system.

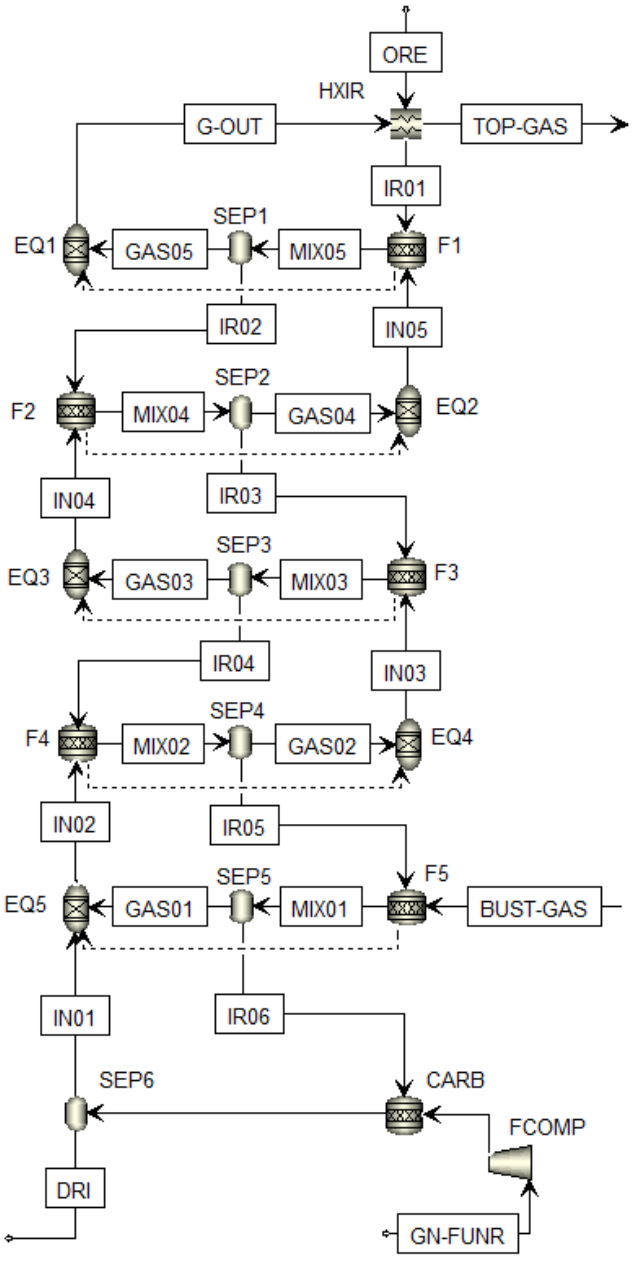

Figure 3-1. Aspen Plus flowsheet of the MIDREX shaft furnace model

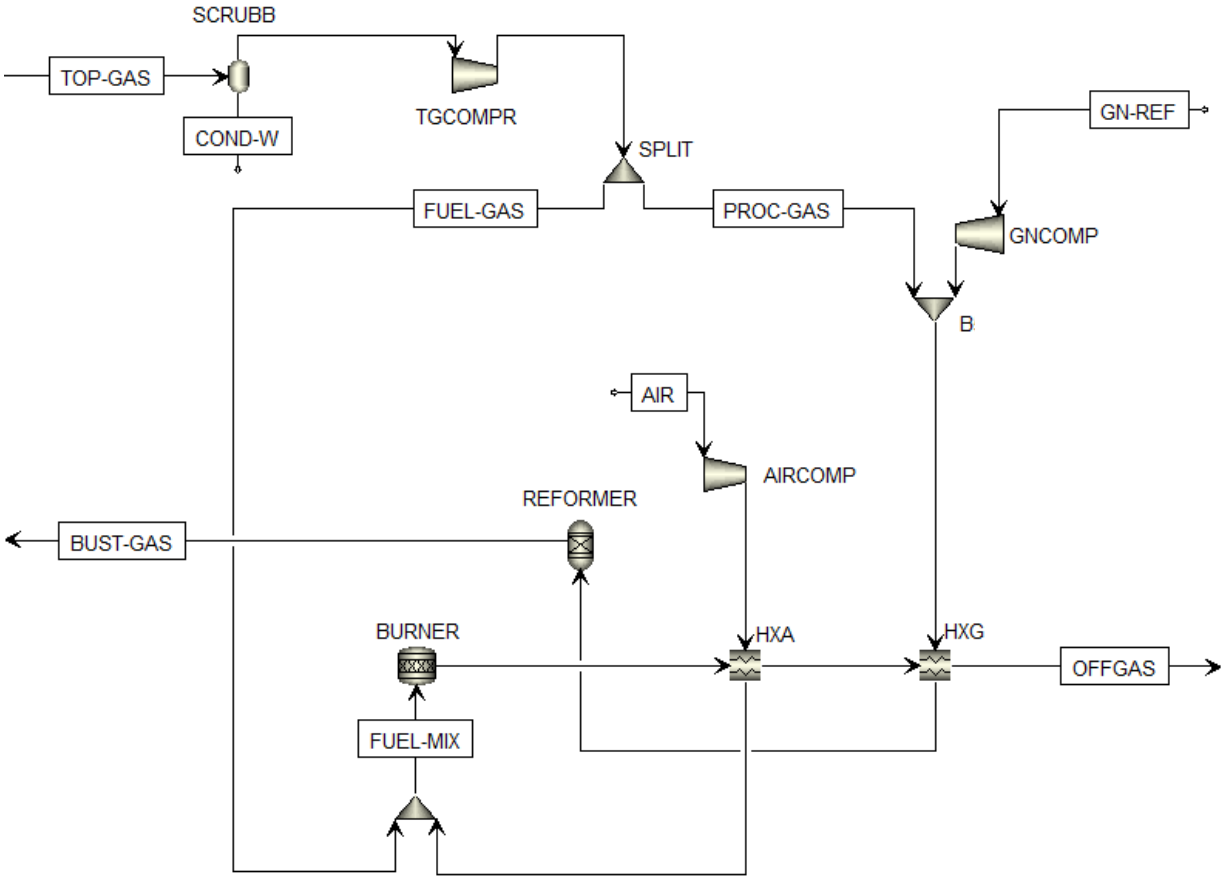

Figure 3-2. Aspen Plus flowsheet of the MIDREX reformer and top gas recirculation

The shaft furnace is implemented as a staged counter-current reactor. The only reduction zone has a representative height of 10 meters [43]. Five reactors, one every two meters of height, are arranged from the top to the bottom, in order to approximate the temperature and the reducing gas concentration profile. In particular, five RStoic reactors F1-F5 are set to reproduce the iron reduction reactions sequence by hydrogen with fixed fractional conversions (Chapter 2, Eq. 11-14), five RGibbs blocks EQ1-EQ5 are set to re-equilibrate in the gas phase the oxygen atoms removed from iron oxides to hydrogen and carbon monoxide at local temperature and pressure. Finally, to have a counter-courrent flow, the solid needs to be separated from the gas phase: it occurs through the separator SEP1-SEP5 in which the solid descends, IR0X streams, and the gas keeps going up, GAS0X streams.

Above the reduction zone, the preheating section is represented by an heat exchanger block MHeatX HXIR that heat up the inlet ore to the target temperature.

Below the reduction zone, carburization is modelled in the reactor RStoic CARB with an injection of natural gas. This reactor increases the carbon content of the solid through the carburization reaction (Chapter 2, Eq. 19).

DRI is discharged downstream of the separator SEP6 and the TOPGAS exits in the upper part. The reducing gas preparation layout follows what has been said in Section 2.1.

The scrubber is represented in two complementary ways: for the whole configuration process, a Flash2 block is used with specified outlet temperature and pressure; in parallel, a RadFrac Column without condenser and reboiler is used only to estimate water make-up and duty, through equilibrium stage calculation.

Reformer is modeled with two reactors. The first, RGibbs REFORMER, is used for the reforming reactions at at specified outlet temperature and pressure; further the restric chemical equilibrium with specified temperature approach is set, in order to simulate the difference between temperature reached at the equilibrium and outlet reactor temperature.

The reformer burners are modelled with the second reactor block, RStoic BURNER, where the fuel mixture, made by split top gas and pre-heated air, is oxidized. The heat released by the burners is linked to the reformer heat required through an Aspen design spec.

Finally, the heat recovery system is modelled with two heat exchangers: one for the air HXA and one for the reformer inlet gas HXG.

The assumptions for inlet streams are reported in Table 3-1, while the main block input specifications are summarized in Table 3-2.

		Value	UoM	Ref.
Iron Ore	Fe_2O_3	97,4	wt%	[44]
	Gangue	2,6	wt%	
	Temperature	25	°C	†
	Flow Rate	120	kg/s	
Natural Gas	CH_4	100	mol%	†
	Temperature	25	°C	
Air	O_2	21	mol%	†
	N_2	79	mol%	
	Temperature	25	°C	

Table 3-1. Inlet stream assumptions for MIDREX Aspen Plus model. † Assumed in this work.

Block		Value	UoM	Ref.
Reformer	Inlet Temperature	580	°C	[24]
	Outlet Temperature	980	°C	[24]
	Pressure Drop	16	kPa	[45]
Burner	Flue Gas Temperature	1050	°C	[45]
	Outlet Pressure	1.02	bar	†
	Thermal Losses	2	$\%_{LHV}$	[46]
Top Gas Compressor	Outlet Pressure	2.8	bar	[47]
	Isoentropic Efficiency	80	%	†
	Mechanical Efficiency	98	%	†
Heat Recovery System	Air Outlet Temperature	650	°C	[48]
	Pressure Drop	0	kPa	†
	Thermal Losses	2	$\%_{LHV}$	†
Shaft Furnace	Iron ore pre-heat Temperature	615	°C	†
	F1 Outlet Temperature	722	°C	†
	F2 Outlet Temperature	749	°C	†
	F3 Outlet Temperature	781	°C	†
	F4 Outlet Temperature	803	°C	†
	F5 Outlet Temperature	821	°C	†
	Methane Conversion	50	%	†
	Pressure Drop	52.7	kPa	[49]
	Thermal Losses	1.8	MW	[50]
Scrubber	Outlet Temperature	55	°C	[47]
	Pressure Drop	5	kPa	†

Table 3-2. Block input specifications of MIDREX Aspen Plus model

The remaining operating assumptions are implemented as control targets using the Aspen tool Design Specification. Each target, taken as assumption, is set as a goal seek by varying a single variable in a reasonable values interval, avoiding overconstrained model, and ensuring a consistent convergence.

The whole design specifications are listed in the Table 3-3.

Design Specification	Target	UoM	Vary
Reducing Gas to Iron Ore Ratio	9	-	Natural gas molar flow at Reformer inlet
Reformer Gas Quality $(H_2+CO)/(H_2O+CO_2)$	10	-	Reforemr Temperature Approach
DRI Discharge Temperature	650	°C	Natural gas molar flow at Furnace inlet
Reformer – Burner Heat Match $Q_{burner}/Q_{reforemr}$	-1	-	Top Gas split to burner
Oxygen excess in flue gases	1	%	Air molar flow inlet
Carbon content in IR06	1	%	Methane conversion in F5

Table 3-3. Design specification adopted for the MIDREX Aspen Plus model

Furthermore, to emulate the gradual conversion of iron oxides along the shaft height, each reactor F1-F5 is set with fixed fractional conversion for the iron ore reduction reactions (Chapter 2, Eq. 11-14). Metallization and carbon content in the DRI are not imposed as target and will be reported as model output in Result section.

3.2.2 H_2 – DRI SOEC Modeling

The Aspen Plus layout of the H_2-DRI configuration with SOEC is presented in the following two figures. Figure 3-3 shows the shaft furnace model, while Figure 3-4 represents the reducing gas preparation through the SOEC and the heat recovery system train.

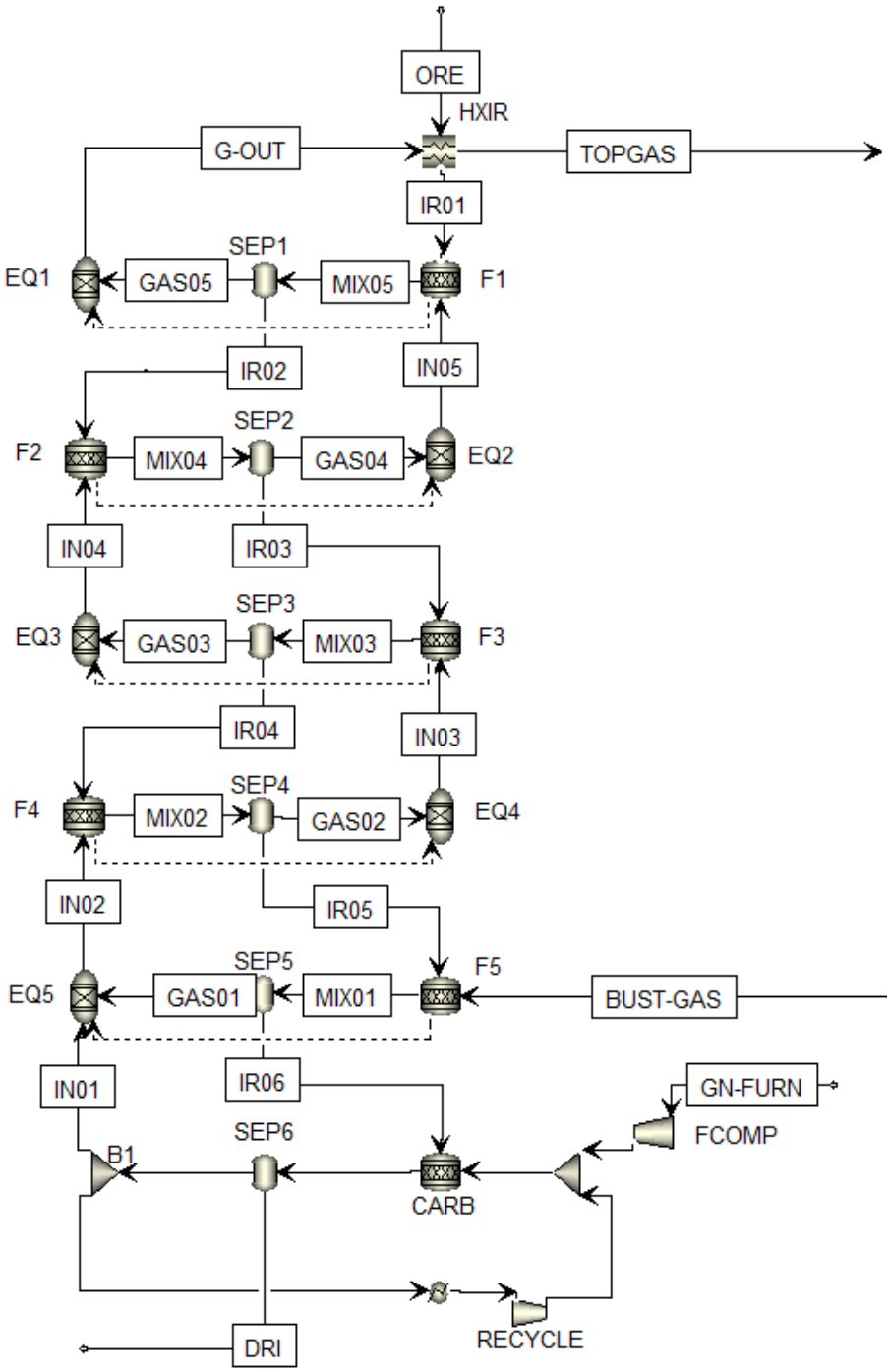

Figure 3-3. Aspen Plus flowsheet for the SOEC H_2-DRI model

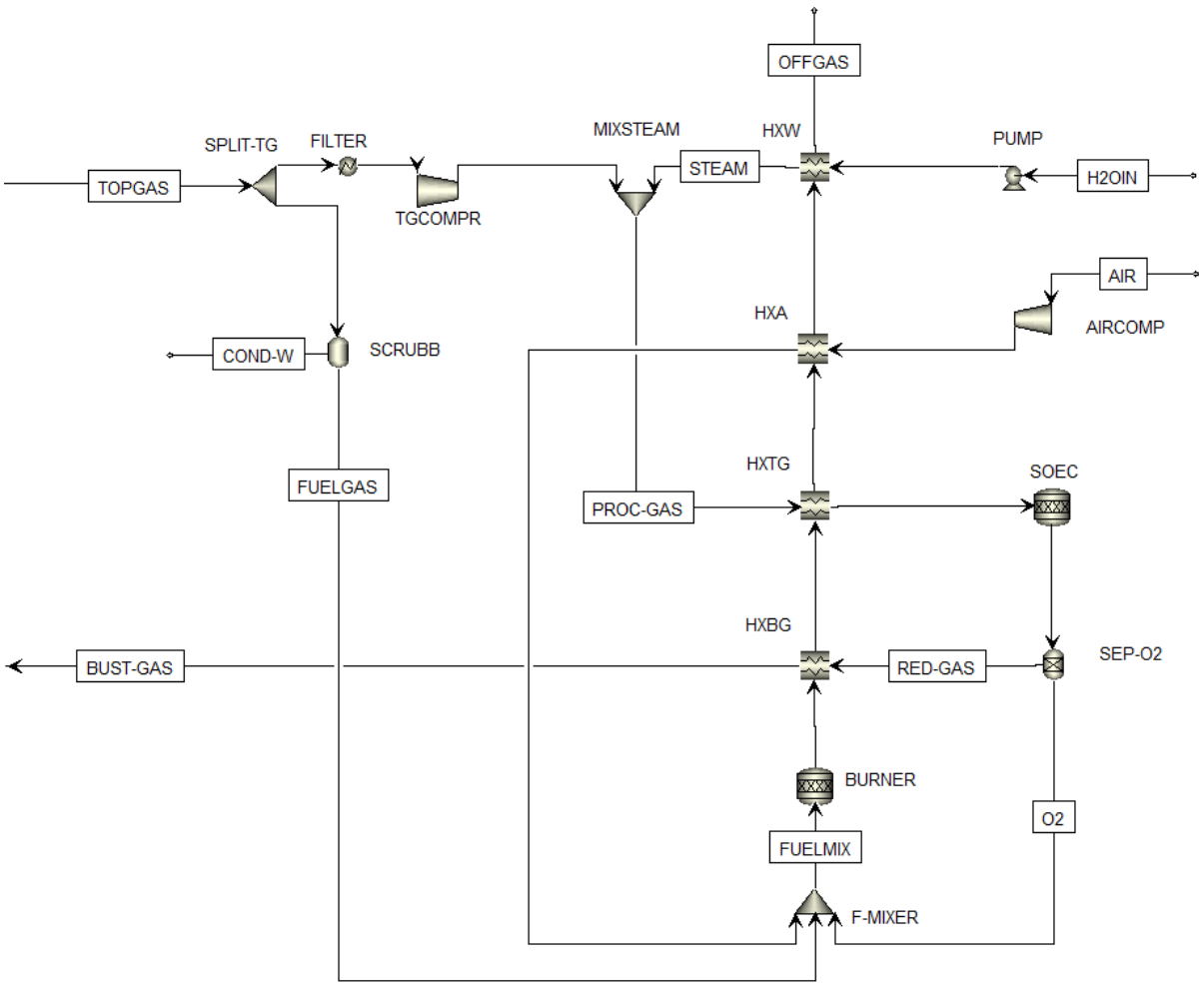

Figure 3-4. Aspen Plus flowsheet of the reducing gas preparation with SOEC

This configuration is implemented starting from shaft furnace: the reducing zone is kept the same as the MIDREX case, while a recycle of the gas products of carburization in the lower section is introduced to limit the injection of natural gas in the furnace.

The reducing gas process, even in this case, follows the description made in Section 2.2. The scrubber, with Flash2 separator at defined outlet temperature and pressure, is modelled only on the fuel gas side, after top gas split; for the process gas a FILTER block is placed to simulate the removal of the small amount of dusts carried from the furnace. The heat recovery system is simulated with four heat exchangers in series, HXBG for the bustle gas, HXTG for the inlet gas of the SOEC, HXA for pre-heated air, HXW for steam preparation. All heat exchangers recover heat released from the flue gases generated in the BURNER, which is set by an adiabatic RStoic where complete oxidation of the species H_2, CO, CH_4 take places. Finally, the SOEC is modelled coupling a RStoic isothermal reactor (SOEC), at the operating temperature and pressure, where the complete reactions take place, and a separator Sep (SEP-O2) where the oxygen flow rate is separated from the exiting stream, emulating the anode side of the cell. The

SOEC is implemented as a simplified block used to compute outlet stream flowrates and compositions consistent with the electrolysis reactions occurring in the electrolyzer.

To ensure a fair comparison with the base case, this configuration adopts the same operative parameter as constraint: the shaft inlet gas temperature and pressure is fixed to the same value; reduced gas quality (RGQ) of the bustle gas is kept identical, the methane conversion in the carburization reactor is set equal to the base case, and iron ore inlet composition is considered the same. For these values refer to the tables in Section 3.2.1.

The remaining assumptions are listed in Table 3-4, while the operating targets imposed by Design Specification are reported in Table 3-5.

Block		Value	UoM	Ref.
Filter	Temperature Change	-10	°C	†
	Pressure Drop	2,5	kPa	†
Scrubber	Outlet Temperature	40	°C	[47]
	Pressure Drop	5	kPa	†
Burner	Duty	0	MW	†
SOEC	Operative Temperature	700	°C	[50]
	Pressure Drop	30	kPa	†

Table 3-4. Block input specification of SOEC H_2-DRI Aspen Plus model

Design Specification	Target	UoM	Vary
Reducing Gas to Iron Ore Ratio	10	-	Water molar flow inlet H2OIN
Reduced Gas Quality RGQ $(H_2+CO)/(H_2O+CO_2)$	10	-	H_2O conversion in SOEC
DRI Discharge Temperature	650	°C	Split fraction in B1
Carbon content in DRI	1,2	%	Natural Gas inlet furnace
Outlet Temperature Burner	1500	°C	Air molar flow inlet
ΔT_{min} in HXTG	50	°C	Top Gas Split
ΔT_{min} in HXAIR	50	°C	Outlet Air Temperature

Table 3-5. Design specification adopted for the SOEC H_2-DRI Aspen Plus model

3.3 Convergence Method

Convergence is obtained by grouping all Design Specifications into dedicated Convergence Blocks and by running the simulation with a written Sequence starting from the TOPGAS stream and proceeding in the sense of the gas loop returning to TOPGAS. The parameters modified by Design Specification are set as initial guess taken from literature data.
This convergence strategy is applied for both configurations.

3.4 Model Validation and Results

The model is validated by comparing the base case Aspen results with published literature data. The validation criteria are to compare key parameters of the cycle: composition of the main streams; the temperature and composition profile of the gas-solid along the shaft height; and finally the metallization degree and the carbon content of the outlet DRI.

		Model Results	Lit. Data	Rel. Error (%)	Ref.
Top Gas	**Composition (vol%)**				[52]
	CH_4	2,71	2,98	9,20	
	CO	20,04	19,79	1,26	
	CO_2	17,00	17,27	1,60	
	H_2	39,94	40,72	1,91	
	H_2O	20,31	19,24	5,60	
Reformer Inlet	**Composition (vol%)**				[45]
	CH_4	18,07	17,29	4,50	
	CO	19,22	20,13	4,54	
	CO_2	16,30	16,12	1,13	
	H_2	38,30	37,53	2,07	
	H_2O	8,11	11,59	30,03	
Bustle Gas	**Composition (vol%)**				[51]
	CH_4	3,7	3,44	8,85	
	CO	34,95	31,95	9,39	
	CO_2	3,62	3,34	8,35	
	H_2	52,55	54,10	2,85	
	H_2O	5,14	7,18	28,45	

	Composition (vol%)			[45]
Flue Gas	CO_2	16,37	16,48	0,67
	H_2O	22,95	21,25	7,41
	N_2	59,71	61,34	2,73
	O_2	0,97	0,93	4,12

Table 3-6. Comparison between main stream composition (wet basis) of Aspen Plus MIDREX model and literature data

Table 3-6 reports the wet basis compositions of the principal streams, i.e. top gas, reformer inlet, bustle gas (outlet reformer) and flue gas at the stack. Since the model assumptions are without Nitrogen (N_2) in the reducing gas loop, the literature data is normalized accordingly.

For the top gas, the largest relative error is on CH_4 (9,20%), yet considering the error in absolute terms, the discrepance is lower than 0,3 vol%, which is considered acceptable. The remaining relative errors average well below the 5%.

For the reformer inlet, H_2O composition shows about 30% relative error. This deviation in water content is driven by the scrubber temperature set-point, which controls the water condensation of the reducing gas. Even in this case the remaining average relative error is around 3%.

Bustle gas seems to have the greater deviation compared to literature data; in this case the key indicator is considered the reformed gas quality (RGQ) at the reformer outlet: Midrex operational plants suggest to maintain this parameter greater than 9,5 [24], with typical value between 10 and 11. With these composition the model plant RGQ remain around 10, consistent value with the Midrex practice.

Finally, the flue gas composition remains below the 5% average relative errors.

Overall, the results obtained on the compositions of the flows are satisfactory.

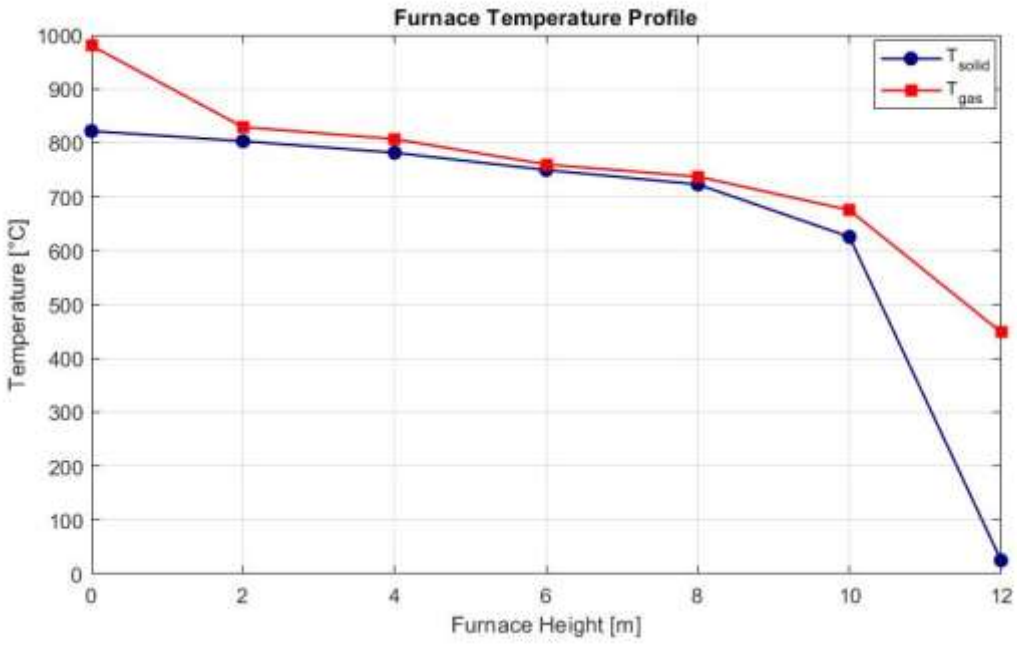

Figure 3-5. Gas-solid axial temperature profiles along the MIDREX shaft furnace Aspen Plus model

In Figure 3-5 the temperature profile along the shaft furnace height is represented. The streams are in counter current: the gas enters the furnace at 980°C and exits at below 450°C, the solid enters at ambient temperature and leaves the reduction zone at about 800°C before the carburization. Across most of the reduction zone, the gas-solid temperature difference is small: in particular the minimum temperature difference is around 10°C, while the average difference is 25°C, not considering the inlets. This trend is supported and validated by literature data, in which gas and solid are nearly in thermal equilibrium along most of the shaft [53].

Further the following figures show the evolution of gas and solid compositions along the shaft height. In particular Figure 3-6 reports the composition of the reducing gas, the left y-axis reports the gas molar fraction on wet basis in vol%, while the right y-axis gives the value of the Reformer Gas Quality.

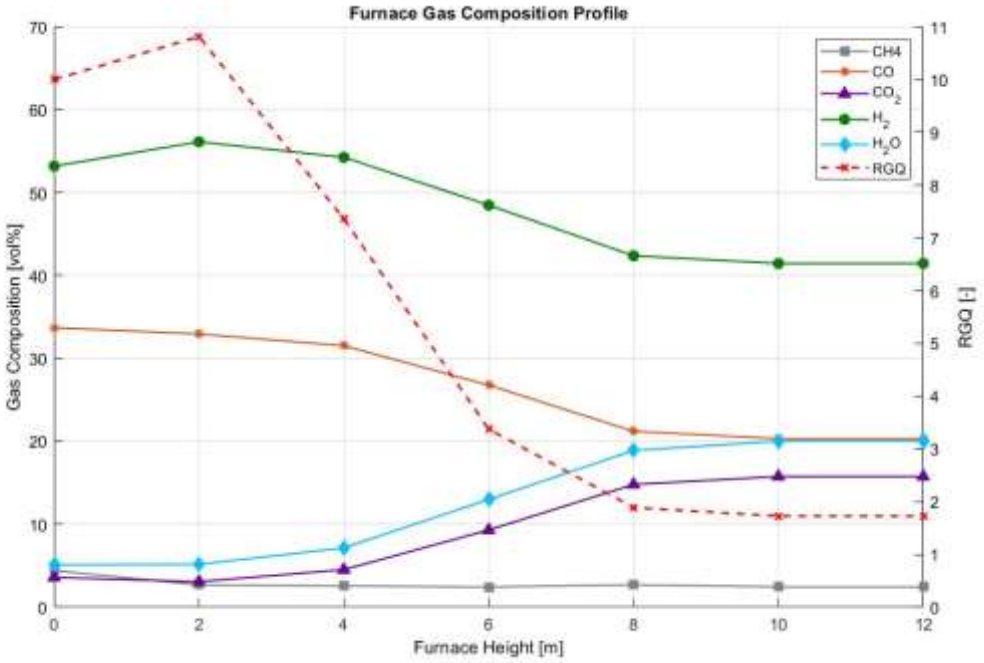

Figure 3-6. Furnace gas composition and RGQ profiles along the MIDREX shaft furnace Aspen Plus model

At the entrance of the reduction zone (at z = 0 m), the gas is rich in H_2 and CO. Moving along the bed, both H_2 and CO decrease, while H_2O and CO_2 increase, consistently with the iron oxide reduction reactions that produce steam and carbon dioxide. About the CH_4, the chart shows a slight decrease over the first meters and then it remains approximately constant; this is because methane reacts with iron mainly in the lower part of the furnace in order to enrich the product in carbon. The small initial increase in H_2 is explained by hydrogen released during the carburization reactions, where it is produced by cracking of the methane. This fraction contributes to add with the incoming gas, raising its concentration in hydrogen.

Finally the dotted line represents the Reformed Gas Quality of the gas. As input data, the gas enters with a quality around 10; and after the small increase due to the enrichment in hydrogen, the parameter tends to decrease to about 2,5-3 confirming the gradual loss in reducing potential of the gas.

Overall the gas concentrations and RGQ are coherent and consistent with the model expectation.

In Figure 3-7 the evolution of the solid along the furnace is shown. The left y-axis reports the iron mass fractions and gangue on wt%, while in the right y-axis carbon content in DRI is given in wt%.

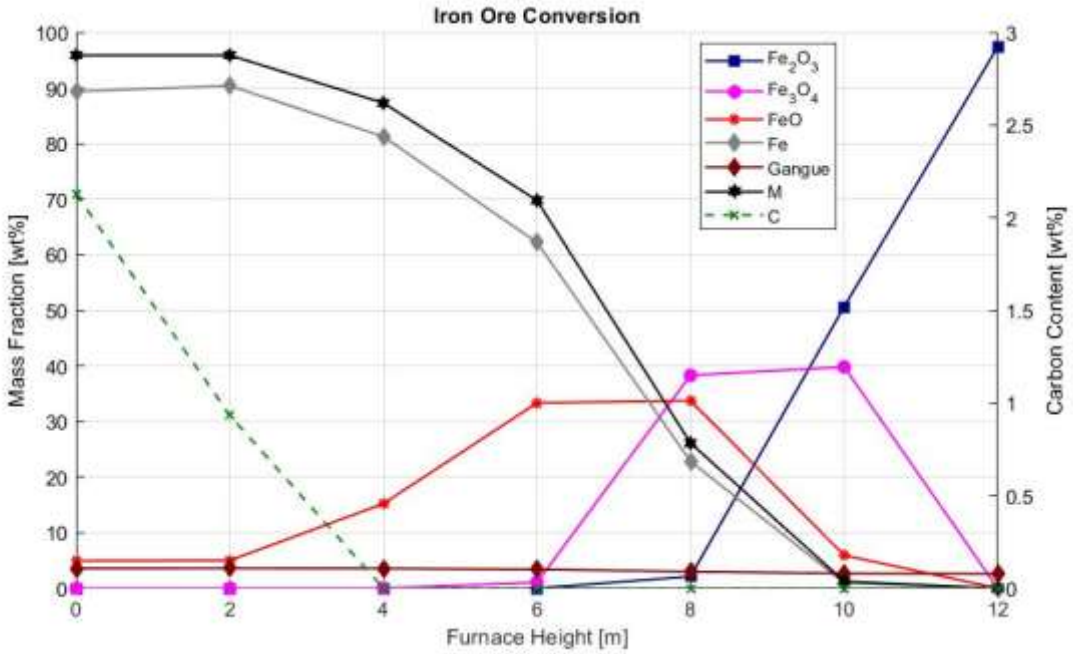

Figure 3-7. Axial profile of iron ore reduction in MIDREX shaft furnace Aspen Plus model

The profile follows the expected reduction sequence. Hematite (Fe_2O_3) is rapidly consumed in the upper section fully converted by around 4 m; Magnetite (Fe_3O_4) is formed with hematite conversion, and disappears after its peak of about 40 wt% at 2-4 m. Wustite (FeO) formation is slightly shifted to the right, meaning in the middle-lower part of the reducing zone, where the temperatures are higher: indeed, according to the Bauer-Glaessener diagram, FeO formation can form only above a certain temperature, around 580°C both with H_2 and CO. Thermodynamically, the step Fe_3O_4 to FeO requires lower reducing potential, given by the ratio $H_2/(H_2+H_2O)$ or $CO/(CO+CO_2)$, than the final step FeO to Fe. This means that a gas able to reduce Wustite to Iron in the bottom section, produces an exhaust gas that is sufficient to reduce Hematite to Wustite. This explains the solid evolution profile along the shaft: Hematite rapidly is converted in favor of Magnetite and Wustite formation in the middle section. Finally in the bottom part, where the temperature and reducing potential are the highest, metallic iron is produced.

As additional check, the simulated solid conversion profile along the shaft is compared with literature profiles reported in Figure 3-8. [54].

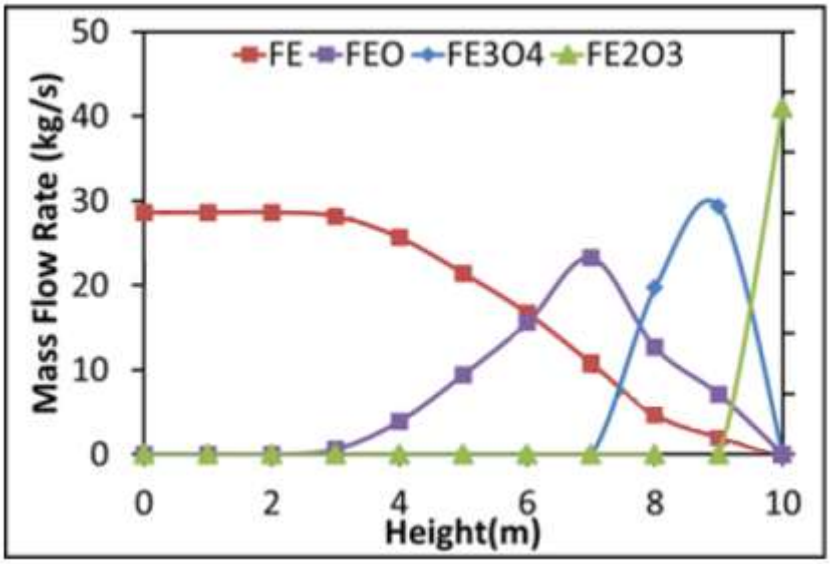

Figure 3-8. Literature solid-phase mass flow profiles of iron oxides and metallic iron along the MIDREX shaft furnace height [54]

The iron species are expressed as mass flow rate, but the trend represents exactly the evolution previously described. Minor differences in peak location are consistent with differences in gas quality and operative temperatures.

Overall, the correspondence supports the validity of the simulated solid phase conversion trend.

Finally, Table 3-7 summarizes the main key performance parameters compared to the typical ranges reported for natural gas Midrex plants in literature data.

Parameter	Value	Range	UoM	Ref.
Metallization ratio	95	92-96	%	[55]
Iron ore	1,37	1.45	t/t_{DRI}	[55]
Natural Gas Consumption	2,31	2,25-2,42	$Gcal/t_{DRI}$	[55]
H_2/CO ratio	1,56	1.5	-	[55]
Carbon content in DRI	2,2	1-3,5	wt%	[55]
CO_2 emissions	453	500	kg_{CO_2}/t_{DRI}	[56]

Table 3-7. Main operating and performance parameters of the MIDREX Aspen Plus model and comparison with reference ranges from literature

Overall, the simulated plant match well the benchmark values; few deviations can be explained by modelling choices. Iron ore consumption results slightly lower than the typical consumption:

this is explained by the low grade of gangue assumed (high quality of pellet), and absence of dust in the furnace.

CO_2 emissions show a small deviation of about 50 kg_{CO_2}/t_{DRI} from literature values, which can be attributed to differences in plant operating conditions and modeling assumptions (natural gas composition, reformer set point, heat losses). Further, downstream EAF emissions are outside the system boundary of this work.

In brief, the table confirms that the model reproduces well an operative Midrex plant; the small deviations are explained by different feed quality and compositions, set-point of the reformer and/or scrubber and heat leakage assumptions, that confirm the validity of the model.

Given this agreement, the validated MIDREX case is used as benchmark for the SOEC configuration, where no further validation is required.

3.5 H_2 – DRI Model Results

This section reports the main results of the hydrogen-based configuration (SOEC case). The shaft furnace and ore feed are the same as in the validated base Midrex case; most set-points are retained, except for the reducing gas to ore ratio (10 vs 9), adjusted for thermal balance, while the reducing-gas generation and make-up streams change.

This adjustment is required to preserve the shaft-furnace thermal profile in the SOEC configuration. Since the SOEC bustle gas is markedly rich in hydrogen, the overall reduction becomes more endothermic; therefore, a slightly higher gas excess provides additional sensible heat and stabilizes the furnace temperature levels along the shaft, avoiding crossover.

Therefore, the model is not re-validate here, but only operative profile of concentration and temperatures, and indicators are presented.

The technical comparison analysis is discussed in section 3.6.

Table 3-8 summarizes wet basis composition for the main streams of the cycle.

	UdM	Top Gas	Inlet SOEC	Bustle Gas
Composition	(vol%)			
CH_4		0,63	0,60	0,60
CO		3,71	3,54	4,89
CO_2		2,83	2,71	1,35
H_2		62,64	59,9	85,4
H_2O		30,18	33,3	7,68
RGQ	[-]	2,01	1,76	10,00
Temperature	°C	489,7	700,0	980,0
Flow Rate	kNm^3/h	687,1	661,6	661,6

Table 3-8. Main gas-stream compositions on wet basis and operating conditions for the SOEC H_2-DRI Aspen Plus model

Consistently with the hydrogen based configuration, the reported streams are rich in H_2 and H_2O. In particular, the bustle gas reaches about 85 vol% in hydrogen with RGQ target of about 10. Hydrogen concentration drops in the shaft furnace in favor of rising of steam, in line with the product of the iron reduction reactions. In the top gas the mixture reach about 30 vol% in H_2O; then, after water make-up, the SOEC inlet becomes richer in steam, about 33 vol%.

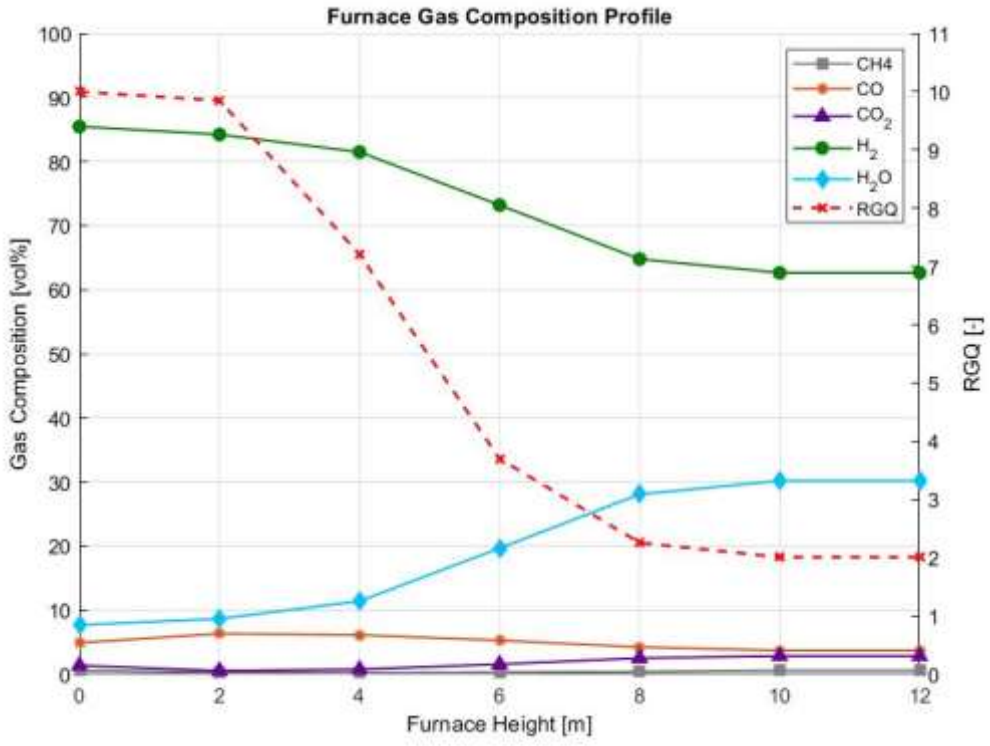

Figure 3-9. Furnace gas composition and RGQ profiles along SOEC H_2-DRI shaft furnace Aspen Plus model

Figure 3-9 reports the evolution of the gas composition along the furnace, the main reducing agent is due to the hydrogen, while the small presence of CO and CO_2 is related to the injection of CH_4 in the carburization zone. This explains the small concentration of CO, which is nevertheless converted to CO_2 along the height. Methane, with its low concentration, remains practically inert in the furnace and even in the cycle loop. The top gas splitter prevents its accumulation in the cycle.

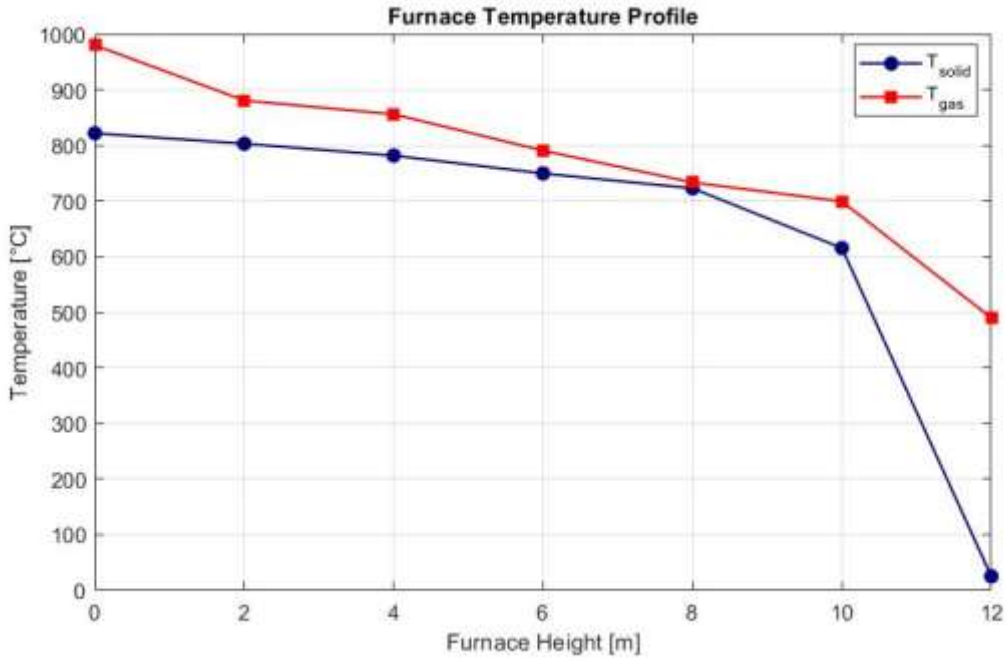

Figure 3-10. Gas-solid axial temperature profiles along the SOEC H2-DRI shaft furnace Aspen Plus model

In Figure 3-10 the temperature profile reflects the same behaviour of the base case with differences in gas temperature that are discussed in the comparison paragraph.

Finally the conversion of iron oxides inside the furnace is reported for coherence, although the conversion on the reactors is set equal in both cases. Figure 3-11 represents the progression of the chemical iron species, showing a difference only in carbon content concentration

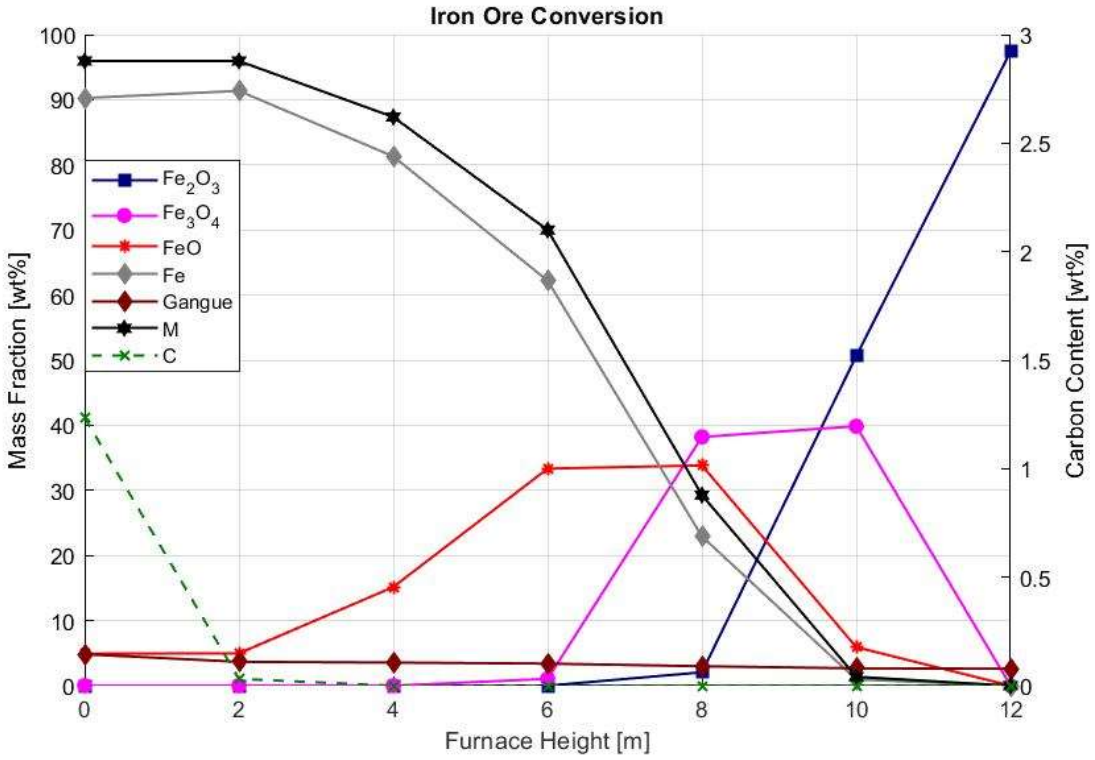

Figure 3-11. Axial profile of iron ore reduction in SOEC H2-DRI shaft furnace Aspen Plus model

The resulting Carbon content in DRI is about 1,2 wt%, since before the carburization zone no carbon is formed inside the iron.

3.6 Comparison

The comparison analysis between the cycles is possible due to the same boundary conditions considered, except the gas to ore ratio. In particular, DRI production rate, furnace inlet gas temperature, bustle gas RGQ and operating pressures are kept constant; in the SOEC case the reducing gas to ore ratio is set to 10 (vs 9 in the base case) to provide additional sensible heat and maintain the furnace temperature profile, as discussed in Section 2.2.2. The remaining variables are obtained from Aspen Plus results.

Focusing on the shaft furnace, modelled identically in both cases, the reducing gas is significantly different in composition. In the MIDREX case, the mixture contains both CO and H_2, so iron oxide reduction is driven by exothermic and endothermic reactions (Chapter 2, Eq 11-19), which keeps the gas temperature profile flatter and with a small gas solid temperature gap. In the H_2-DRI with SOEC configuration the dominant reaction is driven by the hydrogen, which is overall endothermic; the steps continuously absorb heat to sustain the reduction, decreasing the gas temperature. To maintain acceptable temperatures, this case needs more

excess of reductant than the MIDREX case: thus the excess is set about four times the stoichiometric demand, compared with roughly three times in the MIDREX case, evaluated at the inlet of the furnace (bustle gas). The minimum temperature difference is comparable in both cases, around 10 °C on the top of the furnace, while the average temperature differences is much larger in H_2 case (not considering the inlets): 57°C versus 25°C of Midrex plant. Consequently, the top gas temperature is higher in the second case.

Replacing the reformer with the SOEC fundamentally shifts the utilities consumption and introduce internal changes on the cycle. Natural gas use drastically decreases, since the only input is related to the small injection for the iron carburization: the specific natural gas consumption related to the tonns of DRI produced in the H_2-DRI configuration is about 35 Nm^3/t_{DRI}, while in the MIDREX configuration is around 275 Nm^3/t_{DRI}. Conversely, the SOEC needs higher electricity and steam make-up to feed electrolysis; these demands are quantified and discussed in the economic assessment (Chapter 4).

In the H_2 configuration the water condensation is applied only in the fraction of top gas split sent to the burner; the recycled gas in the loop is intentionally kept steam-rich in order to avoid more make-up water. The small presence of dust in the gas, due to the low carbon content, can be removed with a ceramic filter avoiding unnecessary drop in temperature. This choice can reduce the heat duty for pre-heating the process gas to the operating temperature of the SOEC. Overall, although more complex at plant level, since four streams must be pre-heated, the heat recovery system of the H_2 route can benefit from reducing its duty to 450 kW/t_{DRI}, compared with the 640 kW/t_{DRI} of the Midrex case. Then, since the pure oxygen produced by the SOEC is exploited in the combustor, the air consumption necessary for the burner is limited, seeing a value of 0,23 t_{air}/t_{DRI} against the 1,56 t_{air}/t_{DRI} of the base case. Further, another consideration is made on the splitter of the top gas: in the H_2 cycle the quantity requested by the burner in terms of split fraction is less than the base case, respectively 8% and 30%. This is explained by mainly two reasons: the first is the lower amount of heat requested in the heat recovery system; the second is that the split fraction is rich in hydrogen: indeed, once water content is reduced by condensing in the quencher, the drier gas has a higher volumetric LHV; moreover, the fuel rich in H_2 reaches higher adiabatic flame temperature than a syngas rich in CO and H_2. In summary, using pure oxygen and hydrogen rich gas allows to reach the necessary heat duty with a smaller split fraction on the circuit gas, and less inlet air.

Finally, the last consideration is about the comparison of CO_2 emission of the two configurations. One of the main goals of the H_2 route is to cut the most of the emissons at the stack. Considering the almost completely independence from the natural gas, the CO_2 emissions

are drastically reduced for two main reasons: the major one is that the carbon in the gas circuit is almost completely absent, so the total amount of emissions is related to this small fraction of CH_4 and CO, oxidized in the combustion process; then, since the thermal duty is reduced for the heat recovery system, a lower quantity of fuel is burned, leading to less direct CO_2 emission at the stack. Quantifying for both cycles, the direct CO_2 emissions at the stack drop from about 453 kg_{CO2}/t_{DRI} in conventional process to 25 kg_{CO2}/t_{DRI}, corresponding to an almost 95% reduction. In this scenario it is important to consider that only direct emissions are computed, avoiding indirect emissions that could bring the more electricity needed by the SOEC.

Further, the small amount of Carbon inside the loop for the hydrogen based cycle is reflected to a lower carbon content into the DRI: the value results at 1,2 wt% against the 2,2 wt% of the Midrex case. From an operational point of view, too low carbon in DRI can lead to problems to downstream units, especially to EAF (higher power demand, extra carburization). Here, the carbon target is kept at the lower acceptable value to avoid downstream complications while preserving the logic of decarbonization with hydrogen route. Given the product metallization at around 95% a low carbon content in a range of 1,0-1,3 wt% is consistent with the industrial practice and sufficient for the downstream steelmaking process [57].

Table 3-9 summarizes the operating results for both configurations under the shared boundary conditions.

	UoM	MIDREX	H_2-DRI
H_2/CO in Bustle Gas	-	1.58	17.4
Reducing agents/3Fe2O3	-	3	4
$\Delta T_{min, Furn}$	°C	10	10
$\Delta T_{avg, Furn}$	°C	25	57
Natural Gas consumption	Nm^3/t_{DRI}	275	35
Heat Recovery Duty	kW/t_{DRI}	640	450
Air consumption	t_{air}/t_{DRI}	1.56	0.23
Top-gas split	%	30	8
CO_2 emissions	kg_{CO2}/ t_{DRI}	453	25
Carbon in DRI	wt%	2.2	1.2

Table 3-9. Comparison of principal results between MIDREX plant and H_2-DRI configurations

To have a global perspective of the process, an economic assessment is carried out in Chapter 4, which includes an assessment of the total plant costs and a comprehensive analysis of their feasibility and operational ranges.

4 Economic Assessment

This chapter presents the economic assessment of the two DRI production processes investigated in this work, with the aim of highlighting the conditions under which a transition from natural gas to hydrogen based DRI configuration can become economically convenient.

From the technical comparison, the replacement of the reformer with the SOEC produces a deep shift in utilities and emissions: natural gas consumption is drastically reduced, while electricity and steam demands increase to sustain the electrolyzer; CO_2 direct emissions show a drastic decrease, since the only use of natural gas in H_2-DRI route is related to carburization. These modifications lead to a significant variation in investment costs, since different plant components are involved, and in operating costs, due to the different utilities consumption. The economic assessment is designed to determine the overall feasibility of each configuration over its lifetime, and the break-even conditions that define when one configuration is more convenient than the other.

The assessment is developed through a discounted cash flow analysis. Net Present Value (NPV) is adopted as the main index, and the DRI selling price is determined as a break-even value by imposing the NPV at zero at the end of the lifetime considered.

In addition to NPV and break-even price, other complementary economic indicators will be calculated, such as the Levelized Cost of DRI (LCODRI), specific CAPEX and specific OPEX. The analysis also includes climate-economic indicators, as Cost of CO_2 Avoided (CCA) and the Specific Primary Energy Consumption for CO_2 Avoided (SPECCA), in order to quantify the emission reduction in economic terms.

Further, since the two configurations rely on different energy vectors, natural gas and electricity, a sensitivity analysis on these two utility prices is performed, to identify the economic regions of convenience.

A remark on SOEC maturity is required. Solid oxide electrolysis is still in an early industrial scale-up phase and has not yet reached full commercial maturity. Recent assessments classify SOEC as pre-commercial technology, with Technology Readiness Level (TRL) 7-8 [58], with current plants limited to only a few MW in capacity. Consequently, current SOEC costs estimate is affected by high grade of uncertainty and does not represent a fully commercialized system. For these reasons, the H_2-DRI configuration with SOEC is evaluated using a current literature data, representative of early commercialisation, and with long-term 2050 scenario, in

which the technology is assumed to have reached higher maturity with reduced CAPEX and improved performances.

4.1 Methodology

The two configurations are evaluated economically by means of a discounted cash-flow analysis, the break-even selling price of DRI, and the cost of production of DRI, which corresponds to the product value that allows the investment to be fully repaid at the end of its lifetime.

Generally, cash flows represent the annual net balance between revenues from DRI sales and relevant costs associated with the plant. In order to compute these cash flows in a consistent way, a clear estimate of both Capital Expenditures (CAPEX) and Operating Expenditures (OPEX) is required.

4.1.1 CAPEX Estimation

Capital expenditures are evaluated by combining the purchase cost of the main equipment with a set of percentage factors that account for direct and indirect costs associated [59].

The DRI plant is divided into its major sections, identifying the main component (Shaft Furnace, Reformer, SOEC, Heat Recovery System, Auxiliaries etc.), and its purchase cost is determined, by open literature data. When the cost is referred to a different size, the equipment purchase costs, C_i, are computed at the required size, S_i, with cost capacity correlation:

$$C_i = C_{i,0}\left(\frac{S_i}{S_{i,0}}\right)^{n_i} \tag{4-1}$$

where $C_{i,0}$ and $S_{i,0}$ are respectively the reference cost and size, and n_i is the scaling factor.

The resulting equipment costs, referred to a base year, $C_{i,ref}$, is updated to the year 2025 by using the Chemical Engineering Plant Cost Index (CEPCI), by the formula:

$$C_{i,2025} = C_{i.ref}\frac{CEPCI_{2025}}{CEPCI_{ref}} \tag{4-2}$$

The sum of the equipment costs for all the sections of the plant defines the Total Equipment Cost (TEC):

$$TEC = \sum_i C_i \tag{4-3}$$

To the TEC, both direct (DC) and indirect costs (IC) are associated, expressed with a percentage factors. DC refers to the equipment installation, in particular instrumentation and controls, electrical connections, piping, insulation, site preparation and erection works, and are

represented by a single factor f_{DC}. IC are also derived as a percentage of the TEC, and include engineering & head office costs, start-up cost e royalties & fees; all these contributions are grouped into the factor f_{IC}. The of the TEC, DC and IC gives the Total Plant Cost (TPC). Further, an additional margin is introduced to cover design uncertainties and potential cost overruns, expressed through a percentage of TPC with the project contingency factor, f_{PC}. Finally the CAPEX for the considered plant is computed as:

$$CAPEX = (TEC + DC + IC)(1 + f_{PC}) \qquad [€] \tag{4-4}$$

Numerical values adopted for the factors explained are reported in the Economic Assumptions Section (4.2).

4.1.2 OPEX Estimation

In addition to the capital expenditures, the economic performance of the plant depends on the costs required to operate the plant. These costs can be divided into variable production costs and fixed charges [59]. In this work, all these contributions are useful to determine the Operating Expenditures (OPEX), and are evaluated consistently for both configuration studied. Variable operating costs include all expenses that are directly linked to the production of DRI. This type of costs involves expenditures for iron ore pellets, electricity, natural gas and process water, as well as possible costs associated with CO_2 emissions in the form of a carbon tax. All these consumption values are taken from the Aspen simulations for both configurations in a consistent way, and the associated cost C_u is given by:

$$C_u = c_u Q_u \qquad [€/y] \tag{4-5}$$

where c_u and Q_u are respectively the specific cost and the annual consumption of the utilities considered.

All the variable operating costs are computed by summing the single contributions:

$$OPEX_{var} = C_{pellet} + C_{el} + C_{NG} + C_w + C_{C\_tax} \qquad [€/y] \tag{4-6}$$

Fixed charges represent the costs that are not directly related with the DRI production, but rather with the plant size and the component considered. They are represented by three main contributions: operating labour, insurance and maintenance. Labour costs are evaluated from the assumed number of workers required for a plant of the considered capacity and a representative annual salary per person. Maintenance and insurance costs are represented as fixed percentages of the total capital investment, as they depend mainly on the size and capital value of the plant rather than on marginal variations in production. In this work, any catalyst-

related expenses and SOEC stack replacement are implicitly included within the maintenance term. In general, these terms are grouped in the fixed OPEX, given by:

$$OPEX_{fix} = C_{labour} + C_{maint} + C_{ins} \qquad [€/y] \tag{4-7}$$

For each configuration, the Operating Expenditures are obtained as the sum of these variable and fixed contributions, so that:

$$OPEX = OPEX_{var} + OPEX_{fix} \qquad [€/y] \tag{4-8}$$

4.1.3 Net Present Value and Economic Indicators

Once capital and operating costs have been determined, the economic performance of each configuration is evaluated with a discounted cash-flow approach, in line with standard profitability analysis for process plants [59]. The analysis is carried out over the project lifetime, using discrete annual basis. For each year t, an annual Cash Flow, CF_t, is defined as the difference between earnings from DRI sales and expenditure for plant operation and investment.

Since the plant is subject to corporate taxation, both income tax and depreciation of the initial investment have been taken into account.

The annual cash flow in the year t can be written as:

$$CF_t = G_t - Tax_t - CAPEX_t \tag{4-9}$$

where G_t is the Gross Profit and Tax_t is the income tax paid in the year t.

The gross profit is defined as the difference between revenues from DRI quantity, Q_{DRI}, sales at a certain price p_{DRI} and the operating costs in the considered year t:

$$G_t = p_{DRI} Q_{DRI} - OPEX_t \tag{4-10}$$

while the taxable income is calculated on the difference between gross profit and depreciations. Considering the tax rate τ and the depreciation D_t at the yeat t, the tax paid are computed as:

$$Tax_t = (G_t - D_t)\tau \tag{4-11}$$

This formulation provides the after-tax cash flow for each year of the project.

Since the net cash flow is calculated in the year in which it occurred, it is standard practice to discount this value to the reference year in order to account for the time value of money. The net cash flow in each year of the project is brought to its present value at the start of the project by discounting it at some chosen compound interest rate, i.

Therefore, the Net Present Value, NPV, of the project is the sum of the present values of the future cash flows:

$$NPV = \sum_{t=0}^{L_p} \frac{CF_t}{(1+i)^t} \tag{4-12}$$

where L_p is the plant lifetime and t = 0 denotes the first year in which capital is spent.

A positive NPV indicates that the project is economically attractive, while a negative NPV means that the discounted cash flows do not fully cover the initial investment, and the project is not considered economically viable.

In the present work, the DRI selling price is determined as the break-even value that satisfies the condition NPV = 0 at the end of the plant lifetime, which means that the price at which the discounted cash flows over the plant lifetime exactly repay the initial investment and the operating costs under the assumed economic conditions.

In addition to the NPV assessment, a levelized cost indicator is introduced to characterize the overall cost of producing DRI. The Levelized Cost of DRI (LCODRI) represents the average plant cost per tonne of DRI considering both capital and operating expenditures. Capital Expenditures are annualized through the capital charge factor (CCF). The resulting expression is

$$LCODRI = \frac{CCF \cdot CAPEX + OPEX}{Q_{DRI}} \qquad [€/t_{DRI}] \tag{4-13}$$

The CCF is function of the discount rate, i, and the plant lifetime, L_p, defined as:

$$CCF = \frac{i(1+i)^{L_p}}{(1+i)^{L_p} - 1} \tag{4-14}$$

Since this work is centered on the decarbonization of DRI production, it is also important to quantify the cost associated with CO_2 emission reductions. For this reason, the Cost of CO_2 Avoided (CCA) is evaluated by comparing the LCODRI and specific emissions of the two studied configurations:

$$CCA = \frac{LCODRI_{H_2} - LCODRI_{NG}}{e_{NG} - e_{H_2}} \qquad [€/t_{CO_2}] \tag{4-15}$$

This indicator represents the additional cost per tonne of CO_2 avoided when shifting from the natural gas-based to the hydrogen-based process.

Finally, the Specific Primary Energy Consumption for CO_2 Avoided (SPECCA) is used to provide a measure of the additional primary energy consumption for a given reduction in CO_2 emissions. Considering the Primary Energy Consumption (PEC) and specific CO_2 emissions of each configuration, it is defined as:

$$SPECCA = \frac{PEC_{H_2} - PEC_{NG}}{e_{NG} - e_{H_2}} \qquad [GJ/t_{CO_2}] \tag{4-16}$$

These indexes with the NPV analysis provide the basis to assess the techno-economic performance of the MIDREX and H_2-DRI configurations in a decarbonization perspective.

4.2 Economic Data and Assumptions

The economic assessment of both configurations is carried out under a common set of assumptions.

The Capital and Operating Expenditures are evaluated considering a DRI plant reference production of 2.5 Mt_{DRI}/y [50]. For each configuration the starting point of the CAPEX is the TEC of the main process units. In Table 4-1 the equipment considered is listed with its typical size $S_{i,0}$ with the corresponding cost $C_{i,0}$ and the scaling parameter n_i.

Component	**$S_{i,0}$**		**$C_{i,0}$**		**n_i**	**$y_{Ci,0}$**	**Ref.**
Ceramic hot-gas filter	1.466	$kmol_{syngas}/s$	5.900	M€	0.67	2010	[60]
Compressor	10.00	MW_{el}	5.000	M€	0.67	2010	[60]
Desulfuration filter	413.0	MW_{LHV}	660.0	k€	0.67	2010	[50]
Heat exchanger	43.60	MW_{th}	5.200	M€	0.80	2010	[60]
Heat rejection system + BOP	470.0	MW_{th}	49.60	M€	0.67	2017	[50]
Pump	250.0	m^3/h	17.00	k€	0.14	2017	[50]
Reformer	1.000	MW	2.300	M€	0.65	2022	[31]
Shaft Furnace	150.0	t_{DRI}/h	55.00	M€	0.65	2022	[31]
SOEC	1.000	MW_{el}	578.8	k€	0.91	2015	[50]
Venturi scrubber	1.450	$kmol_{syngas}/s$	5.000	M€	0.67	2010	[60]

Table 4-1. Reference costs of main pieces equipment. For the heat exchanger preheating the reducing gas mixture up to temperatures higher than 900 ◦C a material factor of 3.7 has been considered to account for the higher operative temperature

In order to compute the CAPEX a set of percentage factors is assumed (Section 4.1.1). The installation accounts 30% on top of the TEC, while the indirect costs are 22% on top of the TEC, divided into 15% for engineering & head office costs, 5% for start-up costs and 2% for royalties & fees. About project contingency factor, 30% of the TPC has been assumed for the front-end equipment (SOEC), while 20% of the TPC is used for commercially mature components [60].

Decommissioning, recurring capital expenditures, working capital of the steel mill are not included, as they are not expected to significantly affect the relative economic indicators [8].
About OPEX all the operating costs are computed in euro per year, assuming a constant value of money over the plant lifetime (inflation is not included).
Variable operating costs are calculated by the specific utility cost and the Aspen consumption result.
About fixed operating costs, labour cost is estimated from an assumed number of plant workers and a representative annual salary per person, the insurance and maintenance costs are assumed to be 2%/y and 2.5%/y of the TPC, respectively. The only exception is the maintenance cost of the SOEC unit, since this component usually requires the replacement of the stack of electrochemical cells every 6-7 years of operation; thus, for the electrolyzer, a maintenance cost of 14.3%/y of the total direct cost of the single component is assumed.
A summary of the economic assumptions adopted for operating costs, including the specific prices of utilities and the percentages used for fixed charges, is reported in Table 4-2.

Variable OPEX			
Utilities	c_u		**Ref**
Iron ore pellet	100.0	€/t_{pellet}	[63]
Electricity	107.9	€/MWh	[61]
Natural gas	12.89	€/GJ_{LHV}	[62]
Process water	3.700	€/t_{water}	[50]
Carbon tax	100.0	€/t_{CO_2}	[8]
Fixed OPEX			
	Value		
Number workers	150	person	[64]
Salary	75	k€/person/y	[64]
Insurance	2	%/y_{TDC}	[50]
Maintenance plant	2.5	%/y_{TDC}	[50]
Maintenance SOEC	14.3	%/y_{TDC_SOEC}	[50]

Table 4-2. Main assumptions on the variable and fixed OPEX calculation

To calculate the economic feasibility, some financial factors were assumed during the lifetime of the project. The plant lifetime (Lp) is expected 25 years; the plant operates 8000 h annually,

equivalent to 90 % of the maximum capacity. The discount rate (i) is 8 %, in line with typical cost of capital values for the steel industry in advanced economies. A corporate income tax rate (τ) of 20% is assumed, consistent with previous techno-economic studies on DRI and steelmaking routes. This tax rate is applied to the taxable income, defined as gross profit minus depreciation, in the yearly cash-flow calculation.

These financial assumptions are summarized in Table 4-3.

Financial assumptions				
Parameter	**Symbol**	**Value**		**Ref**
Plant Lifetime	Lp	25	years	[50]
Operating hours	h_{eq}	8000	h/y	[66]
Discount rate	i	8	%	[50]
Tax rate	τ	20	%	[65]

Table 4-3. Financial assumption for the cash flow economic cost parameters analysis

4.3 Results

For the base year economic scenario, the techno-economic comparison between the NG-DRI reference plant and the H_2-DRI configuration with SOEC is summarized in the CAPEX and OPEX breakdowns, illustrated in Figure 4-1.

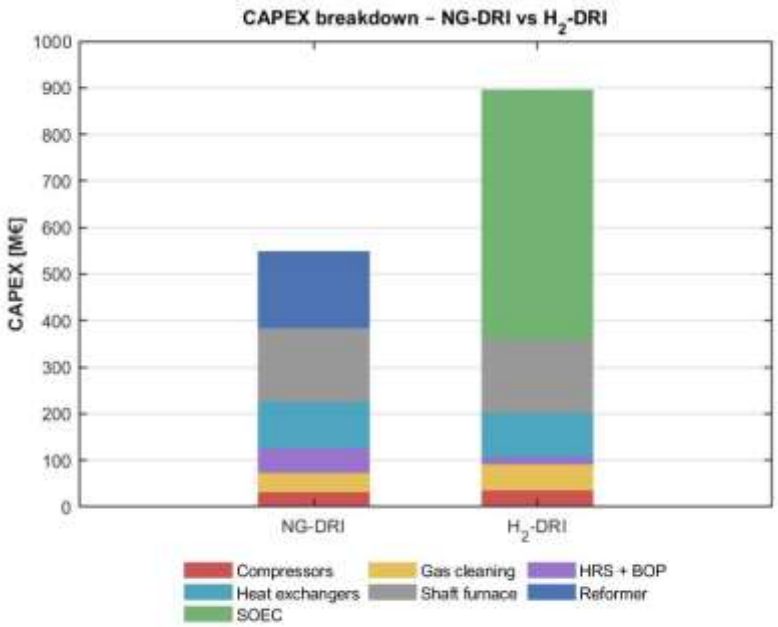

Figure 4-1. CAPEX breakdown: NG-DRI on the left, H_2-DRI on the right

As shown, the NG-DRI route requires a total investement of about 550 M€ for an output of 2.5 Mt_{DRI}/y, correspinding to a specific CAPEX of about 220 €/t_{DRI}/y. When the reformer is replaced by the SOEC system, with the layout adapted to the new configuration, the total investment rise to about 900 M€, that means an increase of roughly 60-65%, with specific CAPEX around 360 €/t_{DRI}/y.

In the NG-DRI configuration, the shaft furnace and the external reformer together account for the largest share of the investment, while compressors, gas cleaning units, heat exchangers and the heat-rejection system (HRS+BOP) contribute with a non-negligible fractions of the total plant cost.

In the H_2-DRI the SOEC represents the dominant capital cost item, accounting for the majority of the total investment, while the shaft furnace investment remains essentially unchanged. The cost of heat exchangers is in the same order in the two layouts, as additional sections are required in the hydrogen case to pre-heat the SOEC feed and to recover heat from hot gases. By contrast, the HRS+BOP section is smaller in the H_2 route since the top gas exiting the shaft

furnace does not need to be cooled down as in the NG route, and the relative equipment is reduced.

These trends are shown in the equipment bar chart of Figure 4-2, and, under that cost assumption (Section 4.2), it highlight that the hydrogen route is almost entirely driven by the high specific cost of the SOEC block, while conventional units and the auxiliary sections remain in a comparable range.

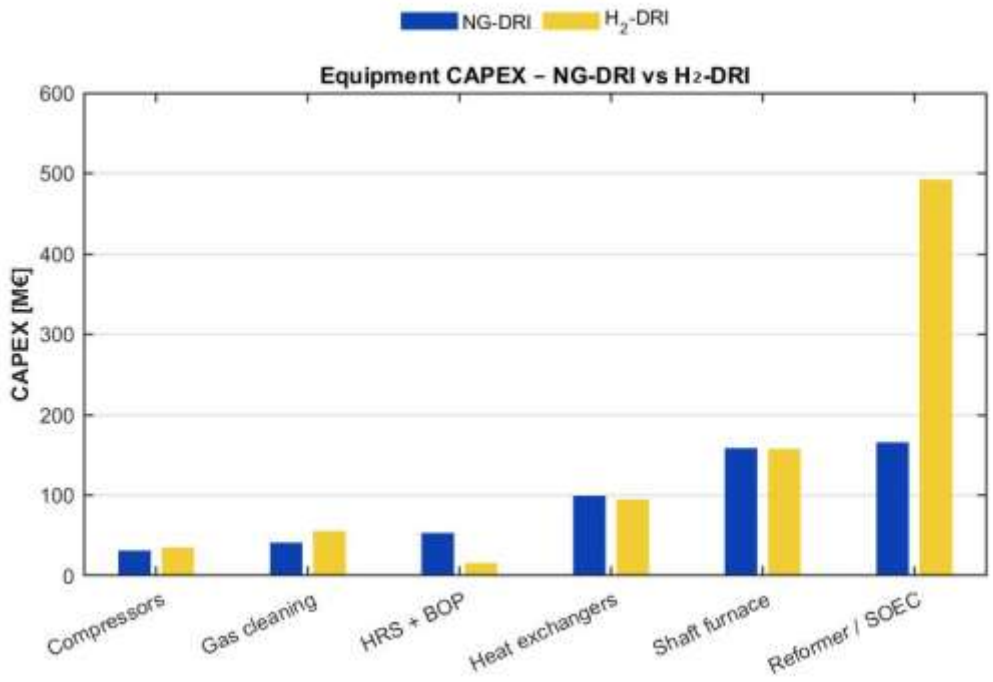

Figure 4-2. CAPEX divided by equipment

Operating expenditures are reported in Figure 4-3. The total annual OPEX of the NG-DRI plant is about 800 M€/y, while the H_2-DRI configuration reaches almost 1000 M€/y, corresponding to an increase of about 25%.

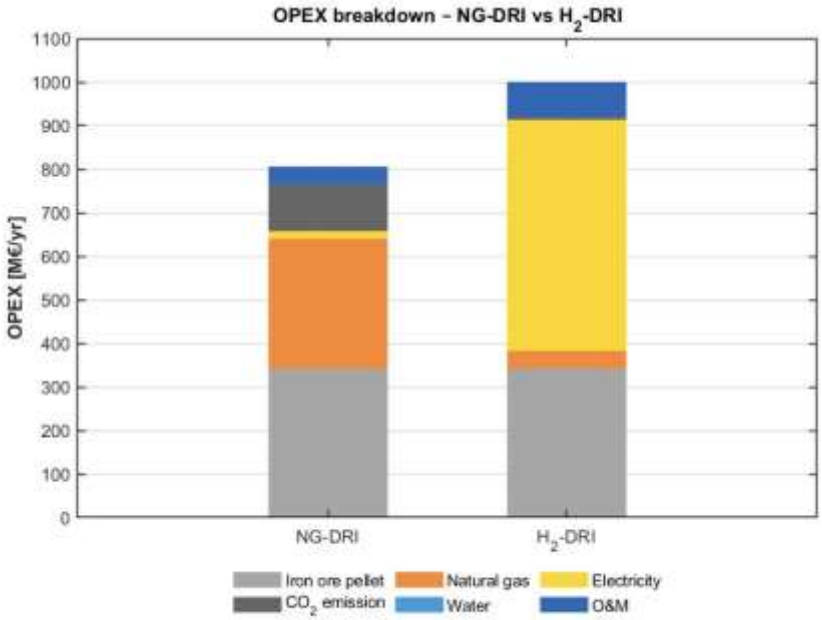

Figure 4-3. OPEX breakdown: NG-DRI on the left, H_2-DRI on the right

In both configurations, iron-ore pellets account for a substantial share of the operating costs (about 42% and 34% respectively of total OPEX). Since the two plants are designed for the same DRI production rate and metallization degree, the absolute yearly expenditure for pellets is essentially the same in both routes. For the NG-DRI plant, the second largest contribution after iron ore pellet comes from natural gas, which together with the carbon tax for CO_2 emissions represents 50% of the related OPEX; electricity and process water represent only 2% of the share. In contrast, the H_2-DRI configuration cost associated to the natural gas is drastically reduced as expected, since its consumption is limited to carburization section, while the electricity demand increases significantly because of the SOEC power requirement. As a result, considering a SOEC power installed of 580 MW, the electricity becomes the main variable operating cost, accounting for 53% of the total OPEX. Instead, the natural gas and carbon tax costs are drastically reduced, showing a decrease of almost 90% compared to the reference case.

Fixed operating costs (labour, maintenance and insurance) represent a relatively small share of the OPEX in both cases, accounting for about 5% and 8% respectively. In absolute terms, however, the presence of the SOEC block introduces an additional charge associated with stack replacement every 6-7 years of operation, which reflects in fixed operating costs for the H_2-DRI route that are almost twice with respect of the reference case.

Figure 4-4 shows the detailed breakdown of annual OPEX divided by categories, for the NG-DRI and H_2-DRI plants.

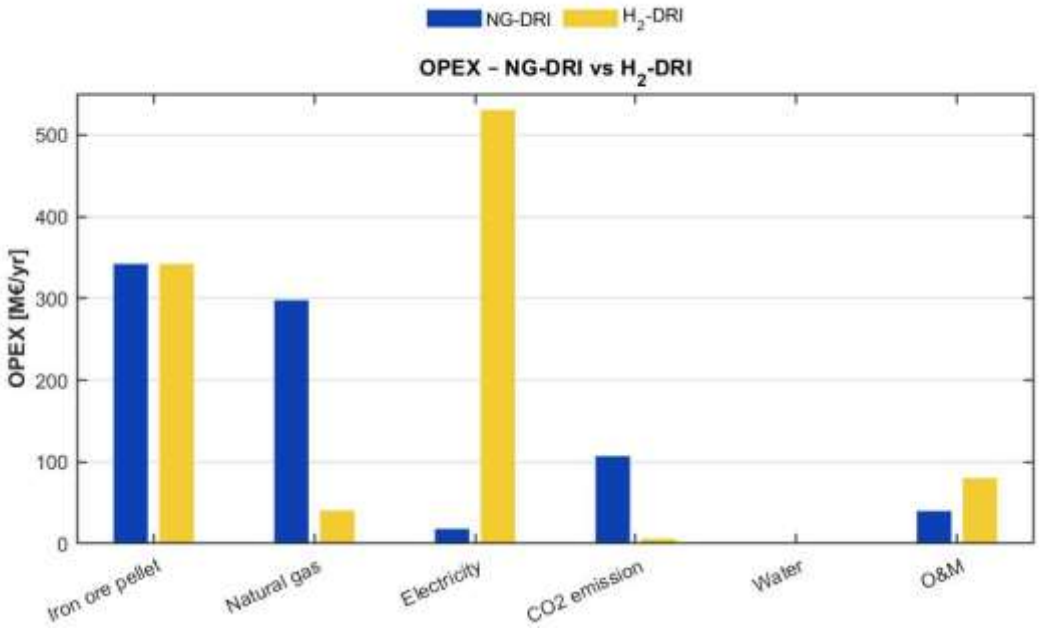

Figure 4-4. Variable and fixed OPEX

Combining the CAPEX and OPEX with financial assumption for the discounted cash flow analysis, the break-even selling price results at 332 €/t_{DRI} and 445 €/t_{DRI} for the NG and the H_2 routes. In parallel with the discounted cash flow analysis, a Levelized Cost of DRI (LCODRI) indicator is evaluated according to the Equation 4-13, accounting to 343 €/t_{DRI} and 438 €/t_{DRI}. On this analysis, the hydrogen route shows an increase of about 28% in LCODRI with respect to the natural gas case. This increase is mainly attributable to the shift from relatively cheap natural gas to more expensive electricity, as well as the higher cost of capital associated to the electrolyzer block.

Shifting to the hydrogen route, the additional cost of CO_2 avoidance, computed by the index CCA (Eq 4-15), is about 234€/t_{CO_2}, a value in the same order of magnitude as literature data in recent techno economic studies. This result is clearly higher than the typical CCA reported for retrofit or incremental mitigation measures on conventional BF-BOF routes, but it is consistent with other deep decarbonization pathways based on hydrogen route.

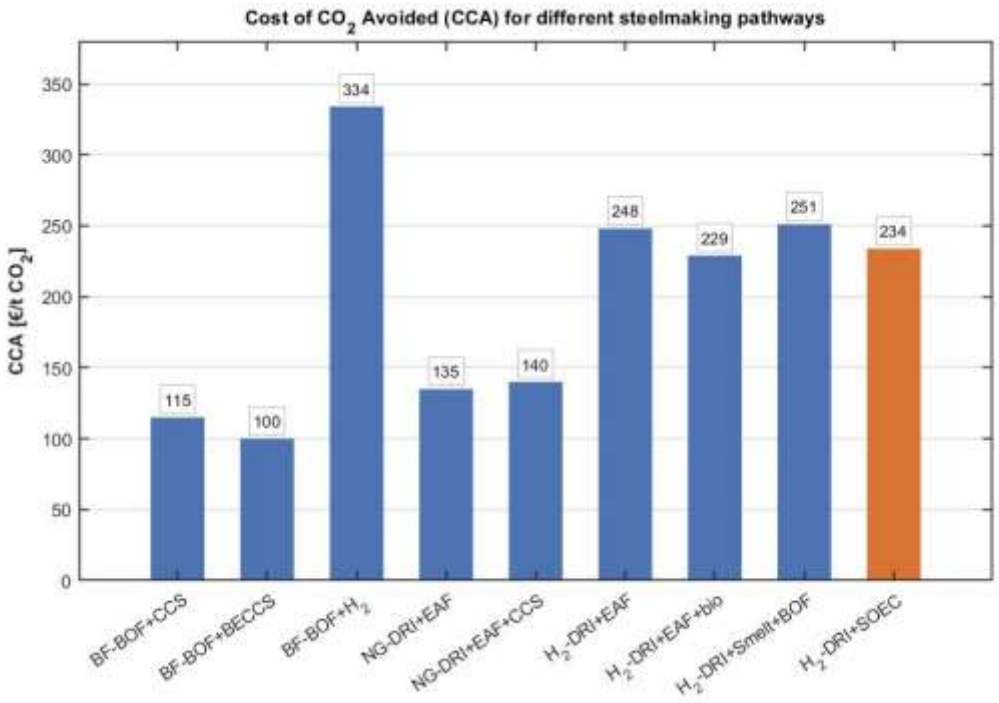

Figure 4-5. Levelized Cost of CO_2 abatement in steelmaking pathways [8]

Finally, using the primary energy consumptions of the two configurations and their specific CO_2 emissions, the resulting SPECCA (Eq. 4-16) is about 16 GJ/t_{CO2}. This means that, on average, each tonne of direct CO_2 emissions avoided with respect to the natural gas reference requires roughly additional 16 GJ of primary energy.

Overall, the base year techno economic evaluation highlights a clear trade-off between production cost and emissions performance. The NG-DRI reference plant emerges as the economically more favourable option, whereas the H_2-DRI configuration requires a noticeably higher capital and operating expenses, resulting in a substantial increase in the specific cost of DRI. In return, the hydrogen route achieves a strong reduction in direct CO_2 emissions compared with the natural-gas case, bringing together high costs of CO_2 abatment and specific primary energy consumption.

Taken together, these results indicate that, with today's technology costs and energy prices, the H_2-DRI configuration is not economically competitive with the NG-DRI route if one looks at cost alone. In practice, it would only become attractive in a context of strong decarbonisation targets, with high carbon prices and developed technologies. For these reasons, Section 4.4 introduces a 2050 scenario and a sensitivity analysis on the main cost drivers, in order to asses under which conditions the hydrogen-based route could become more competitive.

4.4 2050 Scenario and Sensitivity Analysis

In 2050 scenario, both energy markets and electrolyzer technology are expected to be quite different from the actual situation. In Europe these years are characterized by strong variability of natural gas and electricity prices linked to the recent energy crisis and geopolitical tensions, and they are not necessarily representative of a future decarbonized energy system. Long term scenario (SDS, IEA) for steelmaking and ironmaking sectors indicates instead a low carbon power generation, with a progressive reduction of fossil fuels demand and higher carbon prices, in line with the climate goals. On this basis, the 2050 scenario studied is assessed by adopting as central values of the electricity and natural gas the prices suggested in the IEAGHG "Clean Steel" study. For the natural gas a central price of 8.60 €/GJ is assumed, while for the electricity 56 €/MWh [8].

These differences in price lead an important reduction in terms of operating expenses. In fact, compared with the reference year, NG-DRI route shows a moderate decrease in OPEX, roughly from 800 M€/y to 700 M€ (-13.4%), mainly driven by the different natural gas price set; H_2-DRI plant benefits more significantly, with OPEX dropping from about 1000 M€/y to 730 M€/y (-26.9%) as it can exploit cheaper electricity.

This reduction trend is similarly reflected in the LCODRI: in both configurations it decreases, and more important, the gap between them becomes smaller.

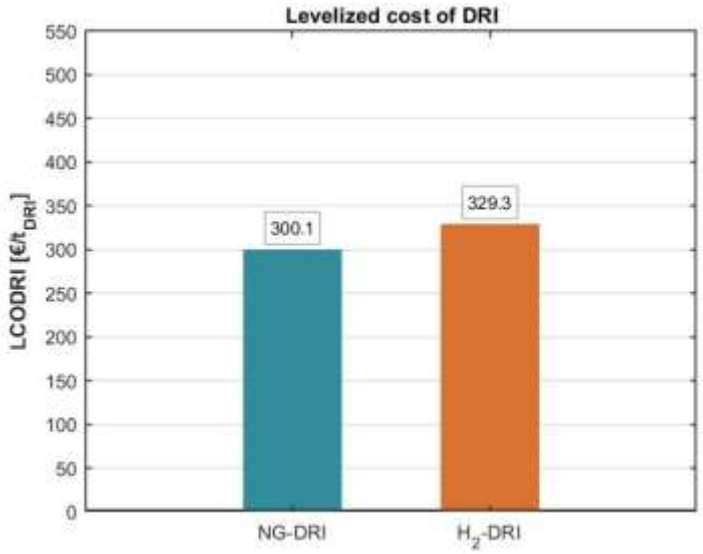

Figure 4-6. Scenario 2050: Cost of DRI production on both routes

As a result, the cost gap of the hydrogen route is reduced from +28% in the reference year, to about +10% in the 2050 scenario, although the NG-DRI configuration still remains the cheapest option at the central values of energy and CO_2 prices.

Since the largest share of the DRI production cost is driven by natural-gas and electricity prices, a sensitivity analysis was performed to assess how different economic scenarios (i.e. variations in natural-gas price, electricity price and carbon-tax level) would affect the economic sustainability of the two configurations.

The results, shown in Figure 4-7, provide a broader picture of the possible market configuration. The LCODRI curves, in the top charts, indicate that the NG route is only weakly affected by the electricity price (reported on the horizontal axis in the range of 20 to 140 €/MWh), while the H_2 route shows a strong dependence on the electricity price. Conversely, the line pattern (solid, dashed, etc.), which represents different natural gas prices, has little effect on the H_2 option but produces a significant increase of the DRI cost in the NG-DRI case.

Further the three different level of carbon tax, from 40 to 160 €/t_{CO2}, moves both sets of curves to higher LCODRI values, but the penalty is much stronger for the NG-DRI option because of its higher direct emissions.

The sensitivity of the Cost of CO_2 Avoided (CCA) is shown in the bottom charts of Figure 4-7, for the same combinations of natural-gas price, electricity price and carbon tax level considered in the LCODRI plots.

Each curve represents the CCA of the H_2 route with respect to the NG reference case for a given natural gas price, as a function of the electricity price. When the CCA value is negative, the hydrogen route is not only less carbon intensive but also cheaper on a levelized cost basis than the NG-DRI plant, so that CO_2 abatement is economically advantageous. The condition CCA = 0 €/t_{CO2} corresponds to the points where the LCODRI of the H_2-DRI route intersects that of the NG-DRI route for the same natural gas price.

As the carbon tax increases, the CCA curves are progressively shifted down: higher CO_2 prices penalize the NG-DRI configuration more strongly, thereby reducing the additional cost per tonne of CO_2 avoided associated with the hydrogen route. At low carbon tax levels and high electricity prices, the CCA remains relatively high and positive, indicating that decarbonization via hydrogen comes at a significant extra cost. Conversely, for higher carbon tax values and moderate electricity prices, the CCA decreases and can approach low or even slightly negative values over a wider range of natural gas prices, reporting operating conditions under which the hydrogen option becomes an economically attractive decarbonisation pathway compared to the natural gas reference.

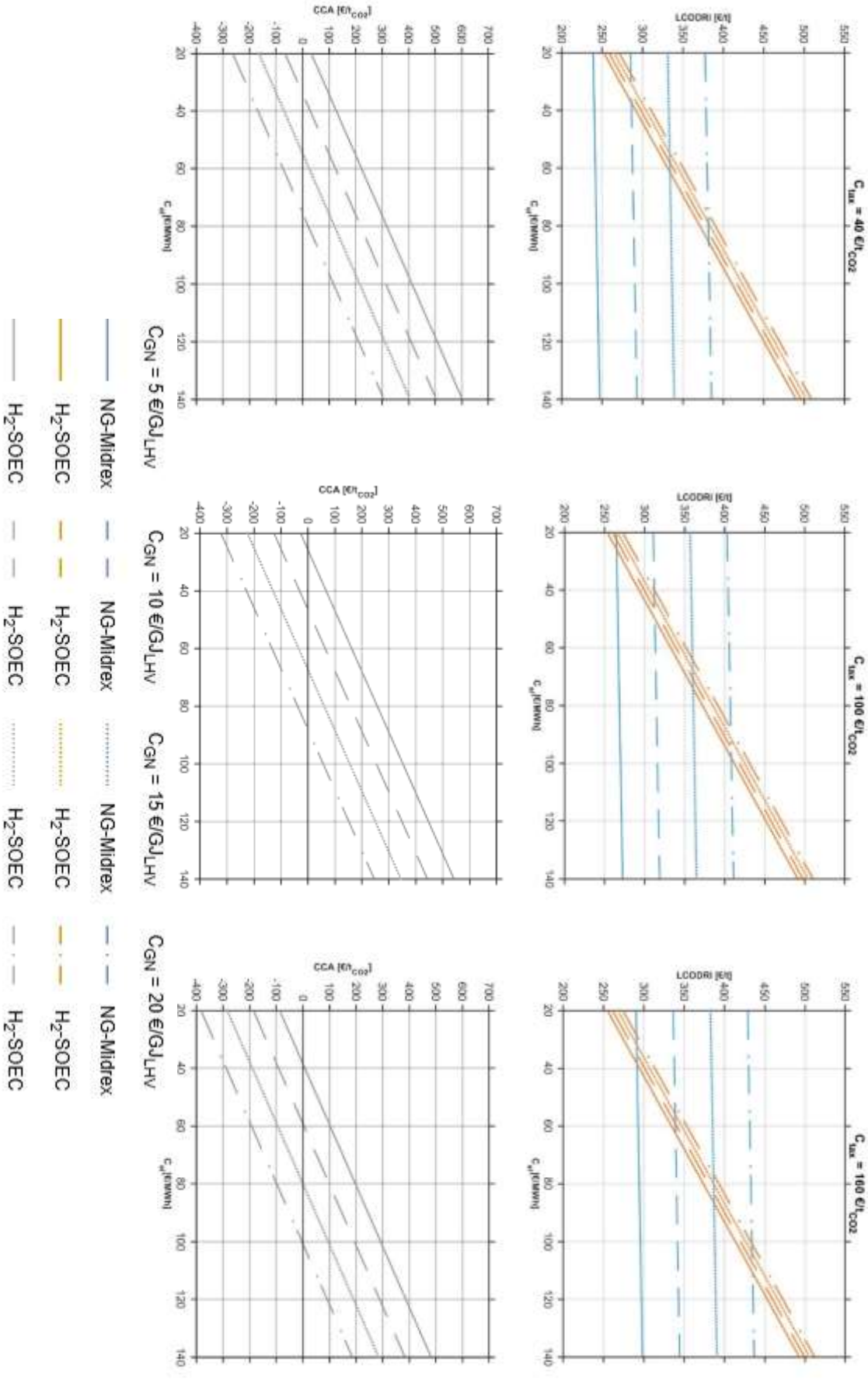

Figure 4-7. Sensitivity analysis by varying the utilities prices

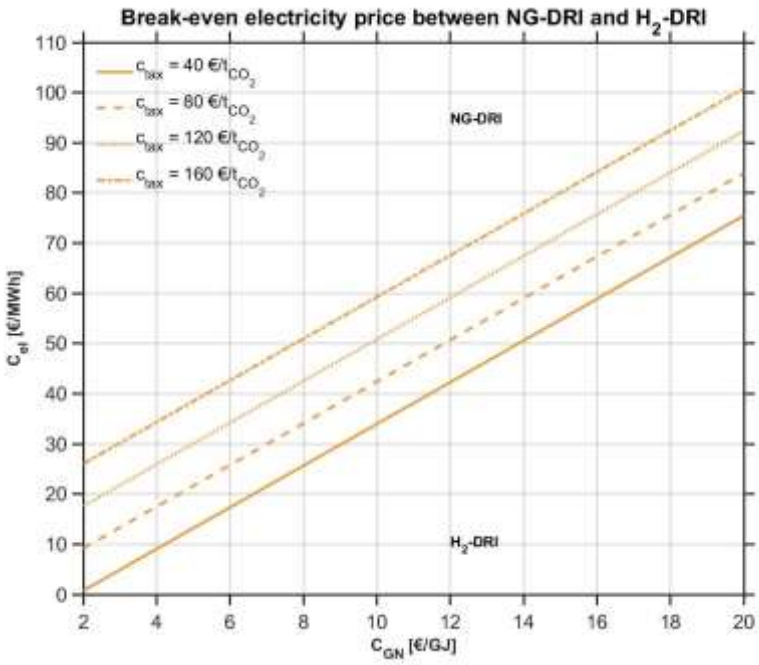

Figure 4-8. Regions of economic convenience for natural gas and hydrogen based DRI production

These combined effects are represented in the breakeven map in Figure 4-8. In this chart the horizontal axis shows the natural gas price C_{GN}, the vertical axis reports the corresponding breakeven electricity price C_{el} for the hydrogen route, and several curves are depicted for different carbon tax values (i.e. C_{tax} = 40, 80, 120 and 160 €/t_{CO2}). Each curve is obtained by imposing the cost of DRI equal in both routes ($LCODRI_{NG} = LCODRI_{H2}$) at fixed carbon tax. In particular, on the curve the corresponding cost of natural gas and electricity gives the same cost of DRI for each route, the points below that curve identify a region in which hydrogen route is more economical than the natural gas reference, while above the line correspond to condition where natural gas configuration has advantageous costs. Increasing the carbon tax, shifts the curves upwards: for a given natural gas price, a higher electricity price can be tolerated while still maintaining cost parity; this means that higher level of carbon tax gives more economic margin to the hydrogen route.

In addition to the utilities prices, the 2050 scenario also assumes technological improvement on the high temperature electrolyzer, leading to a reduction of SOEC installed CAPEX down to 400 €/kW.

The resulting sensitivity of LCODRI is shown in Figure 4-9.

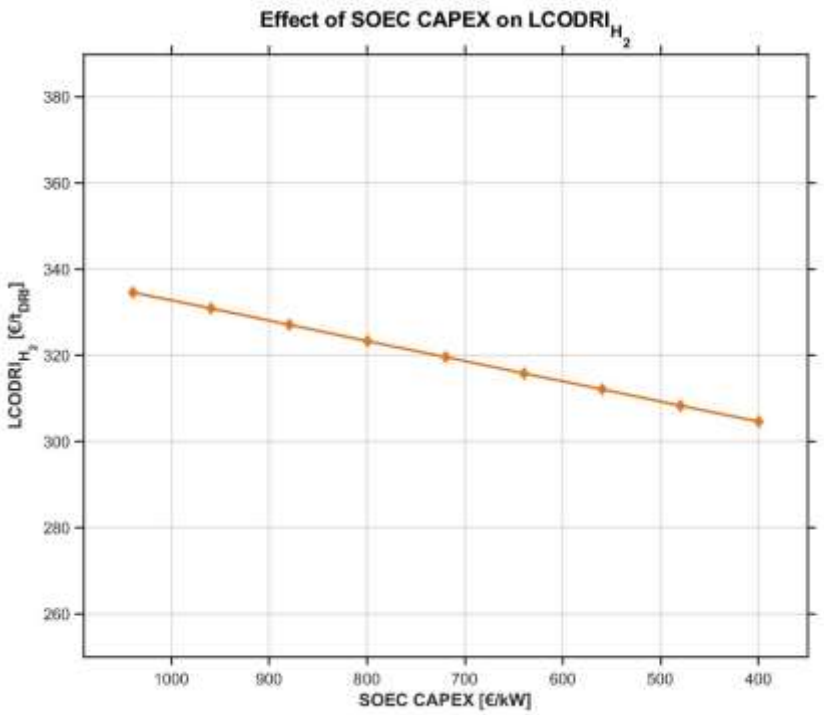

Figure 4-9. Effect of the Electrolyzer CAPEX on the DRI cost

As shown in the chart, the large CAPEX drop, from about 1000 €/kW to 400 €/kW, leads a LCODRI reduction of roughly 30 €/t_{DRI}. This behaviour indicates that the cost to produce a tonne of DRI is principally dominated by utilites costs. In fact, although CAPEX is reduced by 60%, the cost of DRI decreases by only 9%: only a small fraction of the total cost is associated with the annualized SOEC investment.

Finally, to better quantify the relative weight of the different cost drivers, a final sensitivity analysis is carried out around the central scenario of 2050, shown in Figure 4-10. For each main parameter, utilities prices, CO_2 tax and total CAPEX, the LCODRI is computed by varying the reference values in a percentage range, in order to understand its impact on the cost of DRI. The variation is normalized with respect to the reference value and is reported as a percentage value.

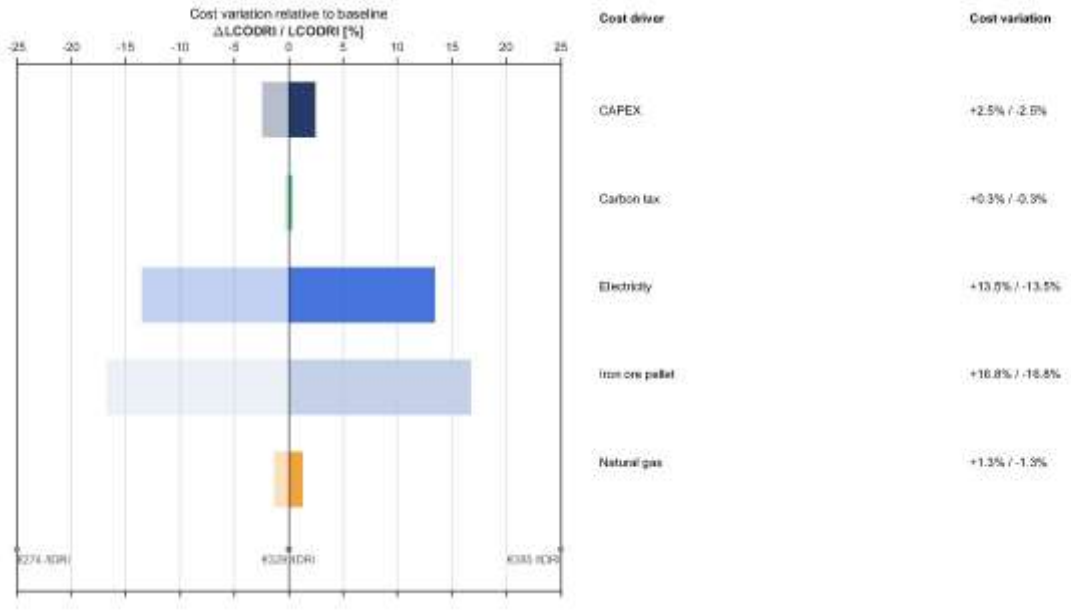

Figure 4-10. Comparision on the major item sensitivity on the LCODRI

The chart confirms that the $LCODRI_{H2}$ is mainly driven by the pellet and the electricity prices: a variation of +/- 40% in these prices produces a variation of +/- 17% and +/- 14% in the cost of DRI. Conversely, the influence of the $CAPEX_{SOEC}$, natural gas price and carbon tax is modest: these items induce changes of few percentage points.

These results confirm that, within the 2050 framework considered here, technology learning on the SOEC and moderate variations of the capital charge alone are not sufficient to alter the economic ranking between the NG-DRI and H_2-DRI routes, unless accompanied by substantial changes in the electricity and/or natural gas prices.

5 Conclusions and Future Developments

The results obtained show that ironmaking decarbonization through hydrogen route with a SOEC is technically achievable and can deliver a clear reduction of direct emissions compared to the natural gas MIDREX reference case, as assessed under shared boundary conditions in Aspen Plus. In particular, replacing the reformer with SOEC electrolysis induces a major shift in the energy vector and in the recycle loop: the specific natural gas consumption decreases from about 275 to 35 Nm^3/t_{DRI} (-87%), while direct stack emissions drop from roughly 453 to 25 kg_{CO2}/t_{DRI} (-95%). This result is achieved at the expense of higher process complexity (more complexity in heat recovery system and more articulated recycle circuit), but maintaining the product specification: the DRI carbon content decreases from approximately 2.2 wt% to 1.2 wt% (-45%), remaining within a range still compatible with downstream use. On the other hand, the SOEC option makes the plant strongly dependent on electricity (installed power of 580 MW), and in this thesis the overall climate benefit was assessed mainly in terms of direct emissions, without explicitly quantifying indirect electricity supply emissions, which may be addressed in future work.

From an economic perspective, the abatement of direct emissions is associated with a marked increase in both investment and operating costs. Total investment rises from about 550 M€ (NG case) to 900 M€ (H_2 case), that is roughly +64%, while annual OPEX increases from approximately 800 to 1000 M€/y (about +25%), with electricity becoming the dominant cost item (around 53% of total OPEX). Consequently, the levelized cost of DRI production increases from around 343 to 438 €/ t_{DRI} (+28%), making the hydrogen configuration economically unattractive under the base year assumptions. Future scenarios and the sensitivity analysis identify regions of potential competitiveness primarily driven by utilities and carbon policy. Under the 2050 central values, the H_2-DRI OPEX decreases more strongly (-26.9%) than the NG-DRI OPEX (-13.4%), reducing the cost gap from roughly +28% to about +10%, although NG-DRI remains generally cheaper at the central point. Moreover, even assuming strong technology implementation SOEC intallation costs (from about 1000 €/kW to 400 €/kW), the LCODRI reduction remains moderate (-9%), confirming that the hydrogen configuration is predominantly OPEX driven. Consistently, LCODRI is most sensitive to electricity and pellet prices (+/- 40% leading to changes of about +/-14% and +/-17%, respectively), while further reductions in electrolyser CAPEX have a comparatively smaller impact. Overall, H_2-DRI with SOEC integration proves highly effective in lowering direct emissions, but its economic

feasibility is mainly conditional on access to abundant and competitively priced low carbon electricity, together with the evolution of pellet markets and sufficiently strong carbon pricing. Future work should therefore extend the boundary from “DRI only” to “DRI to steel” by explicitly integrating the downstream EAF and assessing implications for carbon practice, productivity, and power demand, quantify emissions and electricity system effects to evaluate the full climate benefit of hydrogen based ironmaking and steelmaking, incorporate SOEC real performance over time (degradation, availability, stack replacement, part load and dynamic operation), which can materially affect both annualized CAPEX and OPEX, and investigate hydrogen storage and further heat recovery system and compression optimization to reduce excess of electricity consumption and increase operational flexibility.

References

[1] World Steel Association, World Steel in Figures, Jun. 2025

[2] International Energy Agency (IEA). Iron and Steel Technology Roadmap: Towards more sustainable steelmaking, Part of the Energy Technology Perspectives series, Oct. 2020

[3] World Steel Association, Steel Use by Sector, 2024

[4] World Steel Association, World Steel in Figures, May 2024

[5] World Steel Association, worldsteel Short Range Outlook October 2024, Press Release, Oct. 2024

[6] Reuters, EU steel demand to drop 3.5% in 2022 as energy crisis bites -Eurofer, Reuters, Oct. 2022

[7] SteelRadar, Impact of the Russian-Ukrainian war on the steel industry, SteelRadar, Mar. 2025

[8] IEAGHG, Clean Steel: An Environmental and Technoeconomic Outlook of a Disruptive Technology, Technical Report 2024-02, Mar. 2024

[9] Zuoding, W., Fengman, S., Kuangdi, X. (2022). Blast Furnace Gas, Production and Usage of. In: Xu, K. (eds) The ECPH Encyclopedia of Mining and Metallurgy. Springer, Singapore. https://doi.org/10.1007/978-981-19-0740-1_99-1

[10] World Steel Association, Sustainability Indicators report 2024, Nov. 2024

[11] World Economic Forum, Net-Zero Industry Tracker 2024, Dec. 2024

[12] Genet M., A Transition towards Scrap-based EAFs Continues to Accelerate the Decarbonization of the American Steel Industry, Laplace Conseil, 2025

[13] EUROFER. European Steel in Figures 2024, European Steel Association (EUROFER), 2024

[14] InfraKeys, China's Steel Decarbonization: A New Era of EAF Expansion and Green Steel Opportunities, Jul. 2025

[15] Negri M., Bieker G., Closing the loop: Improving automotive steel recycling for a circular economy, ICCT Policy Brief, Mar. 2025

[16] Wenban M., Global Recycling Day: Analysing the role of scrap in steelmaking through the years, Responsible Steel, Mar. 2025

[17] Midrex Technologies, World Direct Reduction Statistics 2024, Sept. 2025

[18] Atkins P., de Paula J., Physical Chemistry for the Life Sciences, 1st ed. New York: W.H. Freeman and Company, 2006

[19] Shams A., Moazeni F. Modeling and Simulation of the MIDREX Shaft Furnace: Reduction, Transition and Cooling Zones. JOM, 2015 https://doi.org/10.1007/s11837-015-1588-0

[20] Midrex Technologies, Inc., Optimizing DRI production using natural gas, MIDREX NG™ brochure 2018.

[21] Midrex Technologies, Inc., Direct From Midrex: First Quarter 2020, 2020

[22] Bastow-Cox, K. M., Cintron, E. J., & Hughes, G. D. (2021). Direct reduction process utilizing hydrogen. U.S. Patent Application US 20210095354 A1, Apr 2021

[23] Sujay Kumar Dutta., Rameshwar Sah., Direct Reduced Iron: Production. In Encyclopedia of Iron, Steel, and Their Alloys. Taylor and Francis: New York, Mar. 2016, http://dx.doi.org/10.1081/E-EISA-120050996

[24] Kazalski P., Koh P.Y., The Adaptable Midrex® Reformer: A Bridge to the Hydrogen Economy, Sep. 2024

[25] Gavagnin D., Kyrilis E., Estrada Ospino E.J., Spreij M., Postrach S. Refractory lining challenges in transitioning from established to hydrogen-ready operations in DRI shaft furnace technologies. La Metallurgia Italiana (AIM), Apr 2025

[26] Midrex Technologies, Inc. Building DRI Plants: Designed for Today, Engineered for Tomorrow™, 2018.

[27] Midrex Technologies, Inc., Tosyali Algérie sets world production record for a single direct reduction module, Press Release, Jan. 2021

[28] Midrex Technologies, Inc., Direct Form Midrex: Fourrth Quarter 2018, 2018

[29] Midrex Technologies, Inc., Direct Form Midrex: Third Quarter 2018, 2018

[30] Moore C., Levanduski G., Weisenhorn E., Advancing Performance of Nu-Iron's MIDREX® DRI Plant, Tech Article, Mar. 2017

[31] Rosner F., Papadias D., Brooks K. , Yoro K., Ahluwalia R., Autreyd T., Breunig H, Green steel: design and cost analysis of hydrogen-based direct iron reduction, Energy & Environmental Science, Oct. 2023, https://doi.org/10.1039/d3ee01077e

[32] Midrex Technologies, Inc., Getting The Most From Direct Reduced Iron, Direct Form Midrex, Third Quarter 2022

[33] International Energy Agency, The Future of Hydrogen: Seizing today's opportunities, Report prepared by the IEA for the G20, Japan, Jun. 2019

[34] Laguna-Bercero M. A., Recent advances in high temperature electrolysis using solid oxide fuel cells: A review, Journal of Power Sources, Apr. 2012, https://doi.org/10.1016/j.jpowsour.2011.12.019

[35] Institute for Suistainable Process Technology, Next Level Solid Oxide Electrolisis: Upscaling potential and techno-economical evaluation for 3 industrial use cases, 2023

[36] Millet P., Fundalmentals of Water Electrolysism in Hydrogen Production: by Electrolysis, Wiley-VCH, 2015.

[37] Klimeck, R. "Entwicklung einer Fundamentalgleichung für Erdgase für das Gas- und Flüssigkeitsgebiet sowie das Phasengleichgewicht." Dissertation, Fakultät für Maschinenbau, Ruhr-Universität Bochum, 2000

[38] Span, R.; Wagner, W. "Equations of state for technical applications. II. Results for nonpolar fluids." Int. J. Thermophysics, 24 (2003), 41–109

[39] Lemmon, E. W.; Span, R. "Short fundamental equations of state for 20 industrial fluids." J. Chem. Eng. Data, 51 (2006), 785–850

[40] Kunz O, Klimeck R, Wagner W, Jaeschke M. The GERG-2004 Wide-Range Equation of State for Natural Gases and Other Mixtures. GERG Technical Monograph TM15. Düsseldorf: VDI Verlag; 2007. ISBN 978-3-18-355706-6

[41] International Association for the Properties of Water and Steam (IAPWS). Revised Release on the IAPWS Formulation 1995 for the Thermodynamic Properties of Ordinary Water Substance for General and Scientific Use (IAPWS-95). 2018.

[42] AspenTech. Aspen Plus, Physical Property Methods and Models, documentation

[43] Patisson F., Miragaux., Hydrogen Ironmaking: How It Works, Metals 2020, Jul. 2020, https://doi.org/10.3390/met10070922

[44] Lohmeier L., Thaler C., Harris C., Wollenberg R., Schroder H., Briquetting of Fine-Grained Residues from Iron and Steel Production Using Organic and Inorganic Binders, Steel Research International, Vol. 91, Jul. 2020, https://doi.org/10.1002/srin.202000238

[45] Parvathaneni S., Marcelo W.A., CFD Modeling of the Industrial-Scale Bottom-Fired Direct Reduced Iron Reforming Proces, Ind. Eng. Chem. Res. 2024, 63, 27, 11881–11891, https://doi.org/10.1021/acs.iecr.4c01775

[46] Kumara A., Baldeaa M. , Edgara T.F., A Physics-based Model for Industrial Steam-Methane Reformer Optimization with Non-uniform Temperature Field, Computers & Chemical Engineering, Vol. 105, Oct. 2015, https://doi.org/10.1016/j.compchemeng.2017.01.002

[47] Astoria T., Process Gas Heater – Proven Technology for Process Flexibility, Tech Article, Midrex Technologies Inc., Sep. 2019

[48] Midrex Technologies, Inc., Direct From Midrex: Second Quarter 2019, 2019

[49] Jian Xu, Shengli Wu, Mingyin Kou, Kaiping Du, Numerical Analysis of the Characteristics Inside Pre-reduction Shaft Furnace and Its Operation Parameters Optimization by Using a Three-Dimensional Full Scale Mathematical Model, ISIJ International, Vol. 53, May 2013, https://doi.org/10.2355/isijinternational.53.576

[50] Scaccabarozzi R., Artini C., Campanari S., Spinelli M., Techno-Economic and CO_2 Emission Analysis of the Molten Carbonate Fuel Cell Integration in a DRI Production Plant for the Decarbonization of the Steel Industry, Applied Energy 376, Aug. 2024, https://doi.org/10.1016/j.apenergy.2024.124264

[51] Alhumaizi K., Ajbar A., Soliman M.A., Modelling the complex interactions between reformer and reduction furnace in a Midrex-based iron plant, The Canadian Journal of Chemical Engineering 90(5):1120–1141, Oct. 2012, https://doi.org/10.1002/cjce.20596

[52] Hamadeh H., Mirgaux O., Patisson F., Detailed Modeling of the Direct Reduction of Iron Ore in a Shaft Furnace, Materials 2018, Oct. 2018, https://doi.org/10.3390/ma11101865

[53] Marsigny A., Mirgaux O., Patisson F., Operating Solutions to Improve the Direct Reduction of Iron Ore by Hydrogen in a Shaft Furnace, Metals 2025, Aug. 2025, https://doi.org/10.3390/met15080862

[54] Béchara R., Hamadeh H., Mirgaux O., Patisson F., Optimization of the Iron Ore Direct Reduction Process through Multiscale Process Modeling, Materials 2018, Jun. 2018, https://doi.org/10.3390/ma11071094

[55] Gordon Y., Undertanding of Rising and Failure of Gas Based Direct Reduction Processes, Association for Iron & Steel Technology (AIST), 2023

[56] Midrex Technologies, Inc., Direct From Midrex: First Quarter 2024, 2024

[57] Chevrier V.F., Results of Lab Trials of MIDREX ACT™, Tech Article, Midrex Technologies Inc., Sep. 2018

[58] IEA Greenhouse Gas R&D Programme, Comparative analysis of electrolytic hydrogen production technologies with low-carbon (CCS-abated) hydrogen pathways, Technical Report 2024-08, Nov. 2024

[59] Peters M.S., Timmerhaus K.D., West R.E., Plant Design and Economics for Chemical Engineers, 5th ed. New York: McGraw-Hill, 2003

[60] Hannula I., Kurkela E., Liquid transportation fuels via large-scale fluidesed-bed gasification of lignocellulosic biomass, VTT Technical Research Centre of Finland, 2013

[61] Eurostat, Electricity prices for non-household consumers- bi-annual data (from 2007 onwards), nrg_pc_205, Euro*pe*an Commission, https://doi.org/10.2908/NRG_PC_205

[62] Eurostat, Gas prices for non-household consumers-bi-annual data (from 2007 onwards), dataset nrg_pc_203, European Commission, https://doi.org/10.2908/NRG_PC_203

[63] Vogl V., Ahman M., Nilsson L.J., Assessment of hydrogen direct reduction for fossil-free steelmaking, Journal of Cleaner Production, Dec. 2018, https://doi.org/10.1016/j.jclepro.2018.08.279

[64] Nucur Corporation, Nucor Selects St. James Parish, Louisiana, for Iron Making Facility, PRNewswire, Sep. 2015

[65] Xu S., Wang X., Jingqi J., Yu B., Wei Y., Optimum investment strategy for hydrogen-based steelmaking project coupled with multiple uncertainties, Journal of Environmental Management, Vol. 356, Apr. 2024, https://doi.org/10.1016/j.jenvman.2024.120484

[66] Vu, T. T., Seo, J., Kim, E., Ryoo, S. G., Park, B. C., Song, D., Techno-economic analysis of integrated MIDREX process with CO_2 capture and storage: Evaluating sustainability and

viability for iron production, Process Safety and Environmental Protection, Jul. 2024, https://doi.org/10.1016/j.psep.2024.07.005